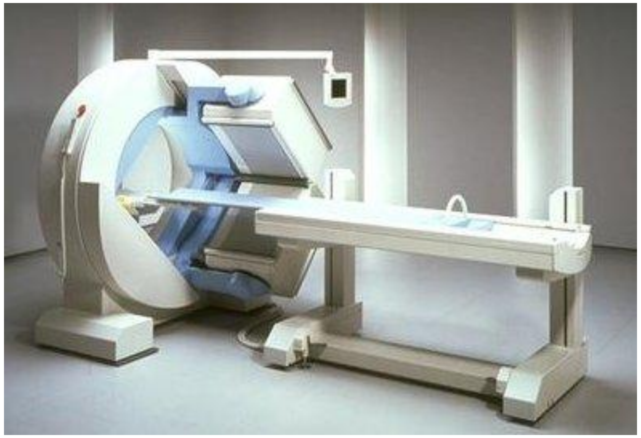

PhD. **Silvano Gnesin**
Institute of Radiation physics (IRA)
UNIL - CHUV

Physics of single-photon emission computed tomography (SPECT)

Master of Science EPF-ETH
Degree in Nuclear Engineering and Medical Radiation Physics

EPFL 23.11.2018

Contents:

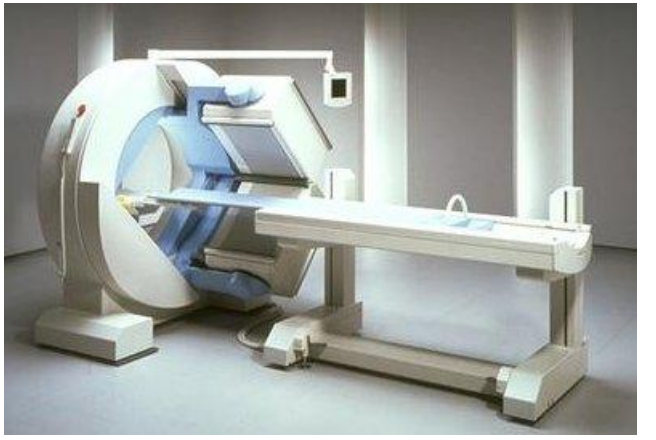

- Principles of Gamma Camera
- Bases of Emission Computed Tomography in nuclear medicine
- Single Photon Emission Computed Tomography (SPECT)

Gamma emission imaging.. a long story

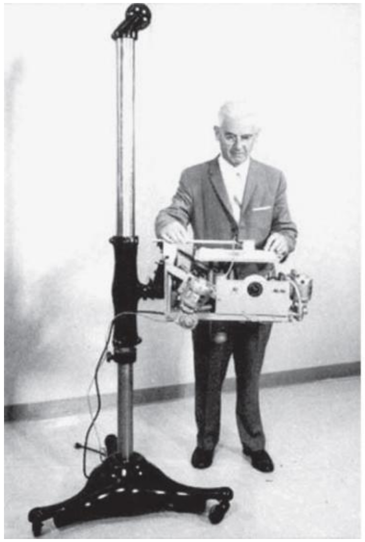

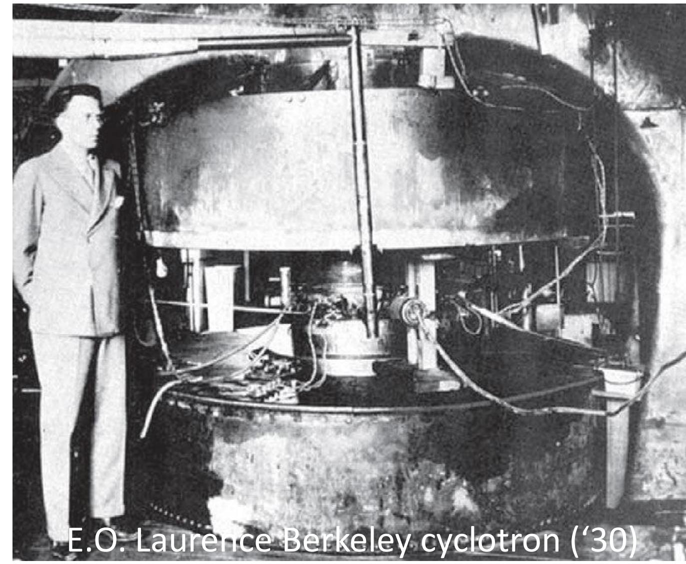

E.O. Laurence Berkeley cyclotron ('30)

Rectilinear scanner 1951
Simple scintillator counter

I-131 Thyroid
Planar imaging

Ink intensity is proportional
To measured photon count-rate

H. Anger 1958
First Gamma Camera
Tc-99m Pertechnetate
Brain scan of a patient with a glioma

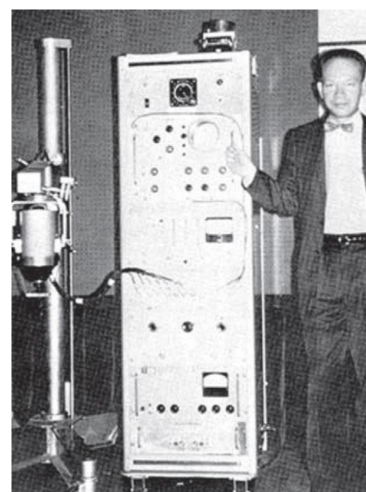

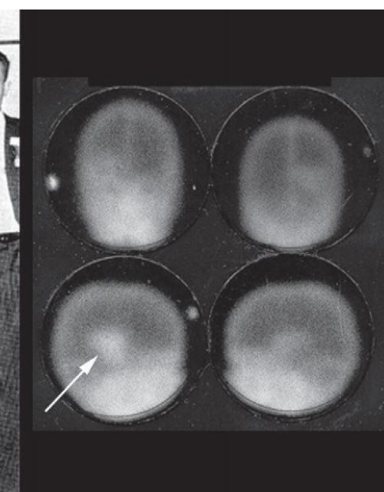

Production of radioisotopes for medical use

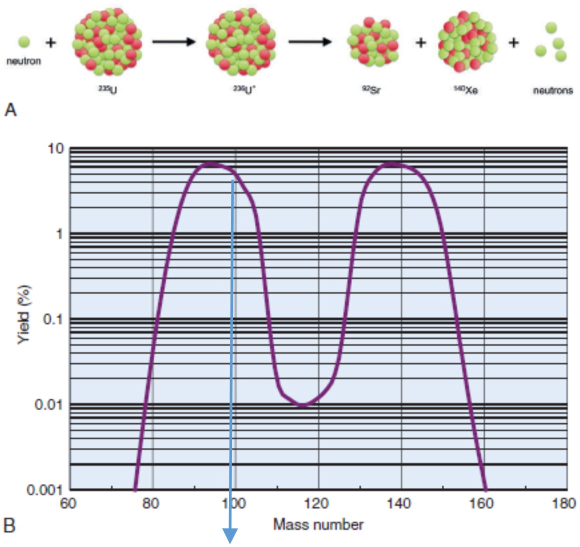

^{130}Te (n,γ) ^{131}Te (β- 25min)→
^^{131}I (β-, γ=364keV 8d)→ ^{131}Xe

^{99}Y (β- 1.5s)→^{99}Zr (β- 21s)→^{99}Nb (β- 15s)→
^{99}Mo (β- 66h)→^{99m}Tc* (γ=140keV 6h)→ ^{99}Tc (stable)

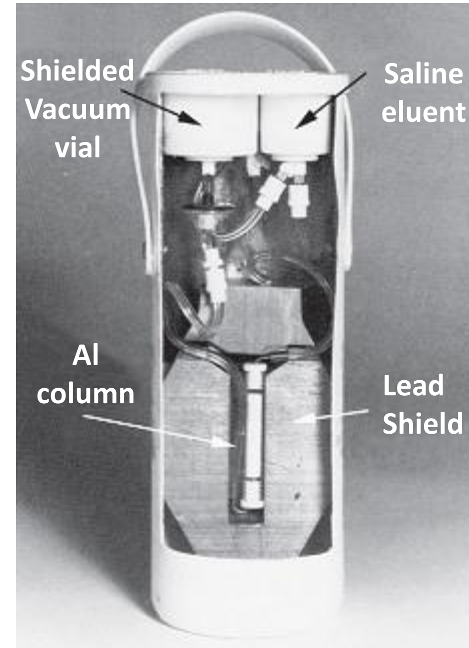

^{99}Mo-^{99m}Tc generator

^{18}O (p,n) ^{18}F
^{109}Ag (α,2n) ^{111}In
^{111}Cd (p,n) ^{111}In

Radio-tracers

The radio-tracer

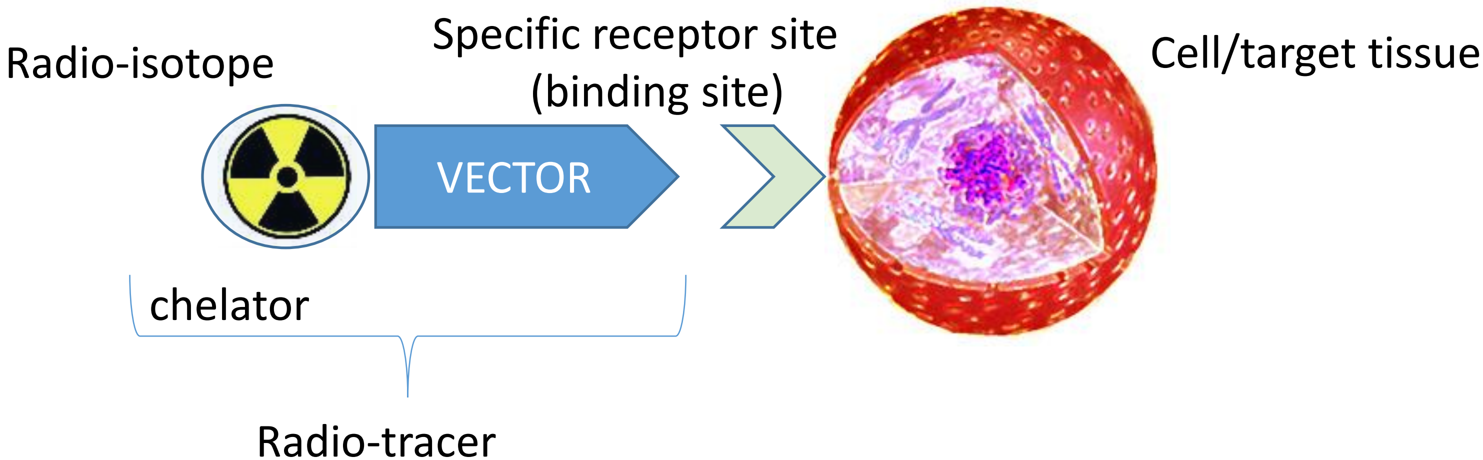

Radio-diagnostic and/or Radio-therapeutic agent

Vectors:

- Molecule (MIBG, DTPA,…)
- Peptide (DOTATATE,…)
- Antibody
- Microparticle (microspheres)

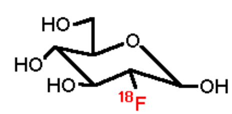

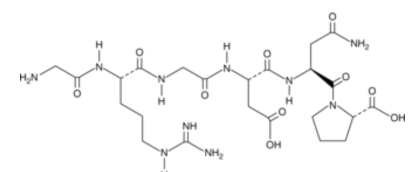

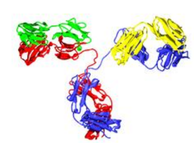

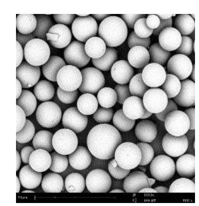

TABLE 1-1

SELECTED CLINICAL NUCLEAR MEDICINE PROCEDURES

Radiopharmaceutical	Imaging	Measurement	Examples of Clinical Use
^{99m}Tc-MDP	Planar	Bone metabolism	Metastatic spread of cancer, osteomyelitis vs. cellulitis
^{99m}Tc-sestamibi (Cardiolite) ^{99m}Tc-tetrofosmin (Myoview) ^{201}Tl-thallous chloride	SPECT or planar	Myocardial perfusion	Coronary artery disease
^{99m}Tc-MAG3 ^{99m}Tc-DTPA	Planar	Renal function	Kidney disease
^{99m}Tc-HMPAO (Ceretec)	SPECT	Cerebral blood flow	Neurologic disorders
^{99m}Tc-ECD	SPECT	Cerebral blood flow	Neurologic disorders
^{123}I-sodium iodide ^{131}I-sodium iodide	Planar	Thyroid function	Thyroid disorders Thyroid cancer
^{67}Ga-gallium citrate	Planar	Sequestered in tumors	Tumor localization
^{99m}Tc-macroaggregated albumin and ^{133}Xe gas	Planar	Lung perfusion/ ventilation	Pulmonary embolism
^{111}In-labeled white blood cells	Planar	Sites of infection	Detection of inflammation
^{18}F-fluorodeoxyglucose	PET	Glucose metabolism	Cancer, neurological disorders, and myocardial diseases
^{82}Rb-rubidium chloride	PET	Myocardial perfusion	Coronary artery disease

MDP, methylene diphosphonate; MAG3, mercapto-acetyl-triglycine; DTPA, diethylenetriaminepenta-acetic acid; HMPAO, hexamethylpropyleneamine oxime; ECD, ethyl-cysteine-dimer; SPECT, single photon emission computed tomography; PET, positron emission tomography.

Production of radioisotopes for medical use

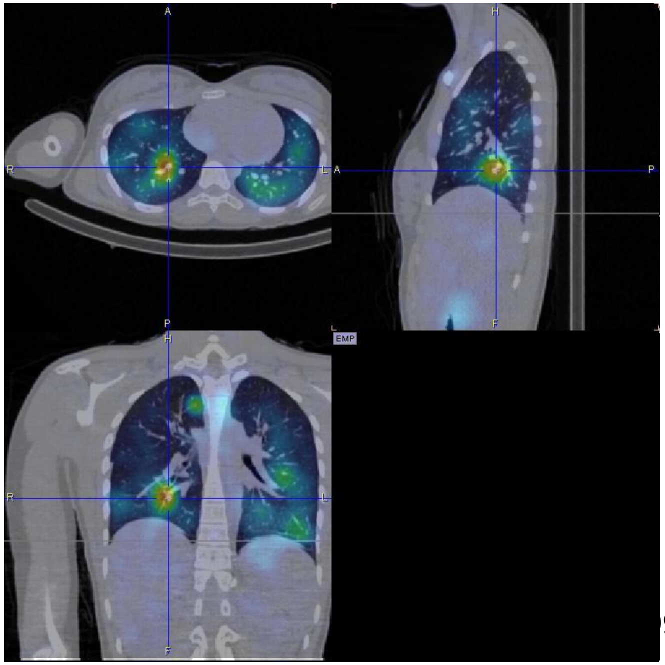

$^{130}Te\ (n,\gamma)\ ^{131}Te\ (\beta^-\ 25min) \rightarrow$

$^{131}I\ (\beta^-, \gamma=364keV\ \ 8d)$ $\rightarrow\ ^{131}Xe$

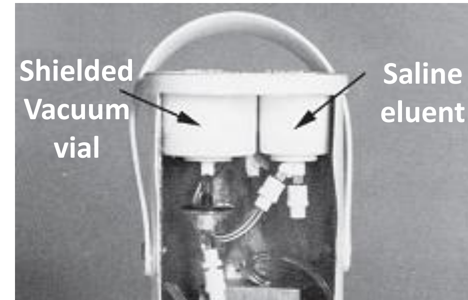

$^{9}Nb\ \ (\beta^-\ 15s) \rightarrow$

$^{99}Mo\ \ (\beta^-\ 66h) \rightarrow$ **$^{99m}Tc\ (\gamma=140keV\ 6h)$** $\rightarrow\ ^{99}Tc$ (stable)

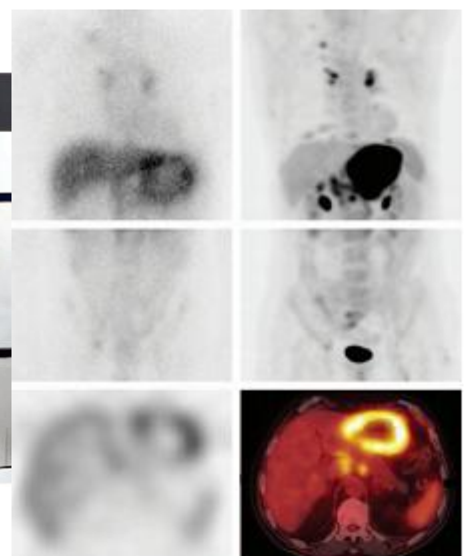

$^{18}O\ (p,n)$ **^{18}F**

$^{109}Ag\ (\alpha,2n)$ **^{111}In**

$^{111}Cd\ (p,n)$ **^{111}In**

The gamma camera
Introduction to basic principles

Gamma camera: main components

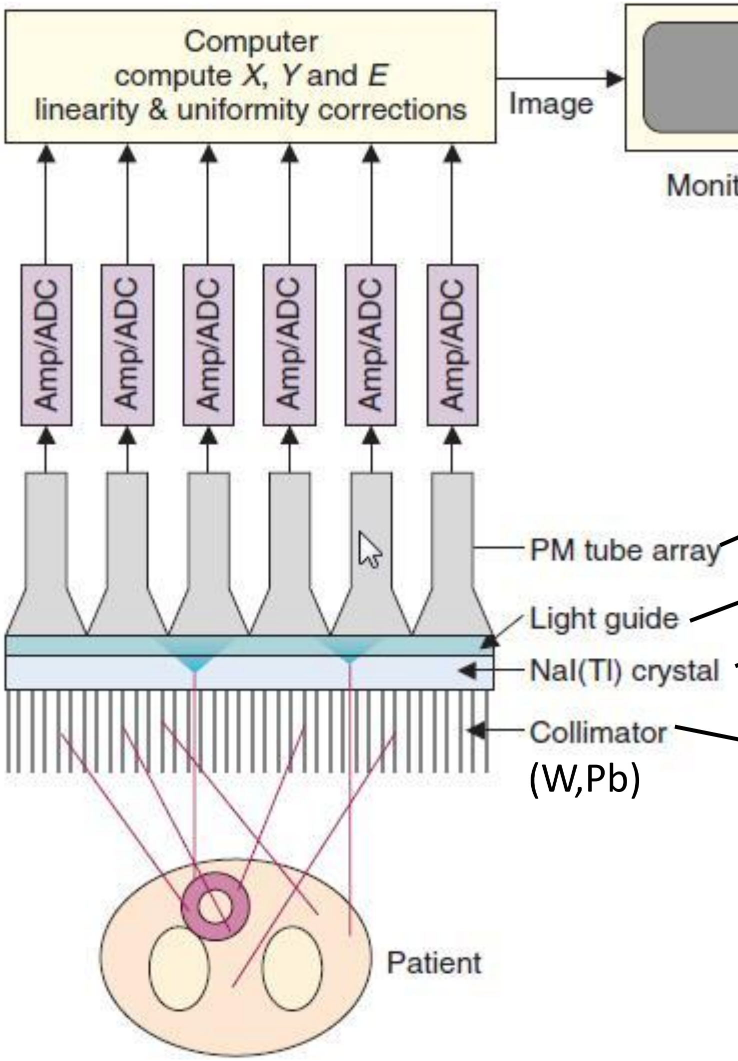

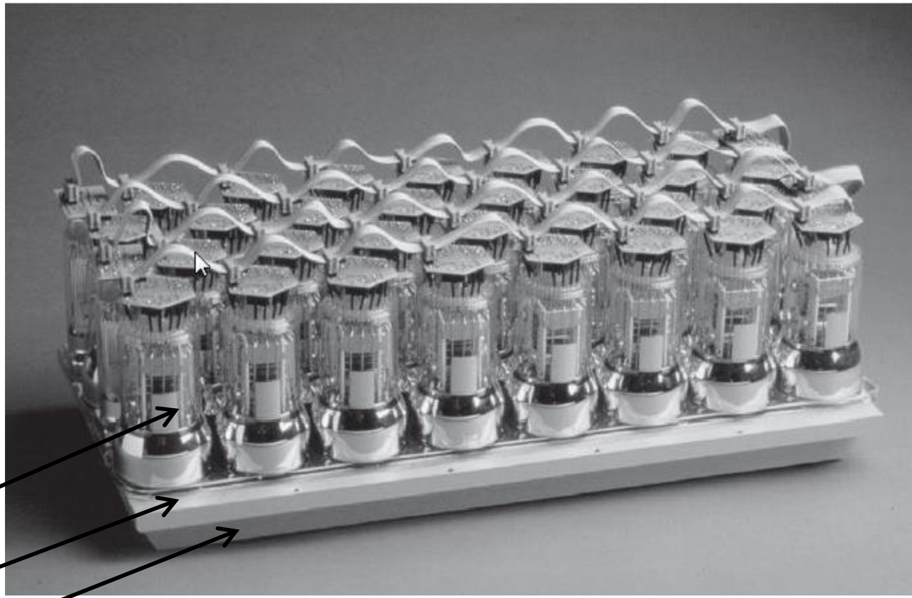

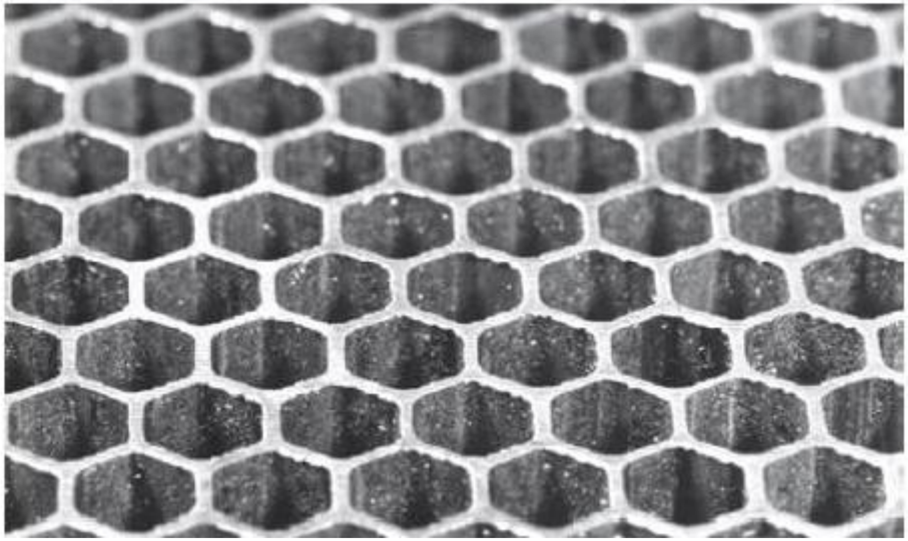

Parallel hole collimator

Emission imaging is based on scintillation detection

Emission imaging is based on scintillation detection

Scintillation material
- Organic (liquids)
- Inorganic (crystals NaI, BGO, LSO)

The amount of emitted light (visible) is proportional to the deposited energy

Property	NaI(Tl)	BGO	LSO(Ce)
Density (g/cm^3)	3.67	7.13	7.40
Effective atomic number	50	73	66
Decay time (nsec)	230	300	40
Photon yield (per keV)	38	8	20-30
Index of refraction	1.85	2.15	1.82
Hygroscopic	Yes	No	No
Peak emission (nm)	415	480	420

^{99m}Tc Eγ=140 keV → Photon yield = 38 x140 = 5320

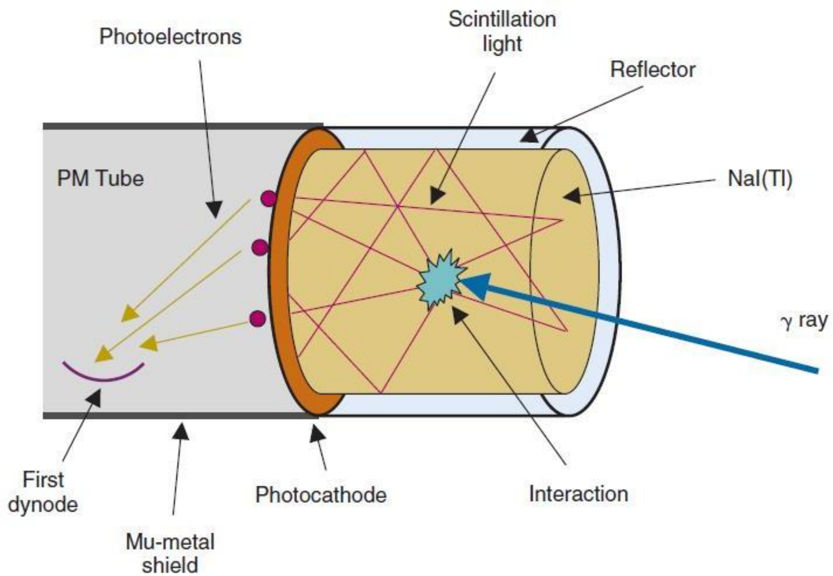

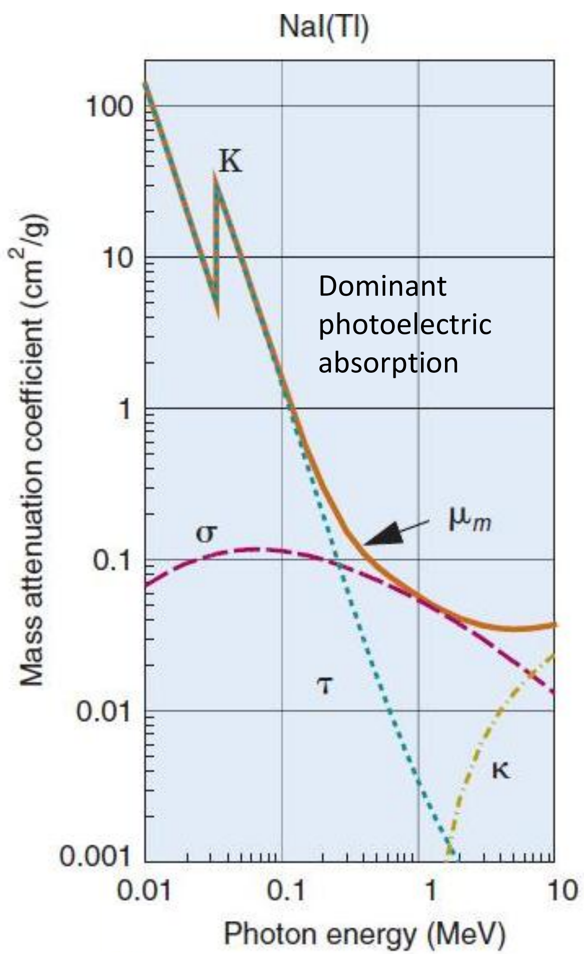

Gamma camera: Problems in event localization

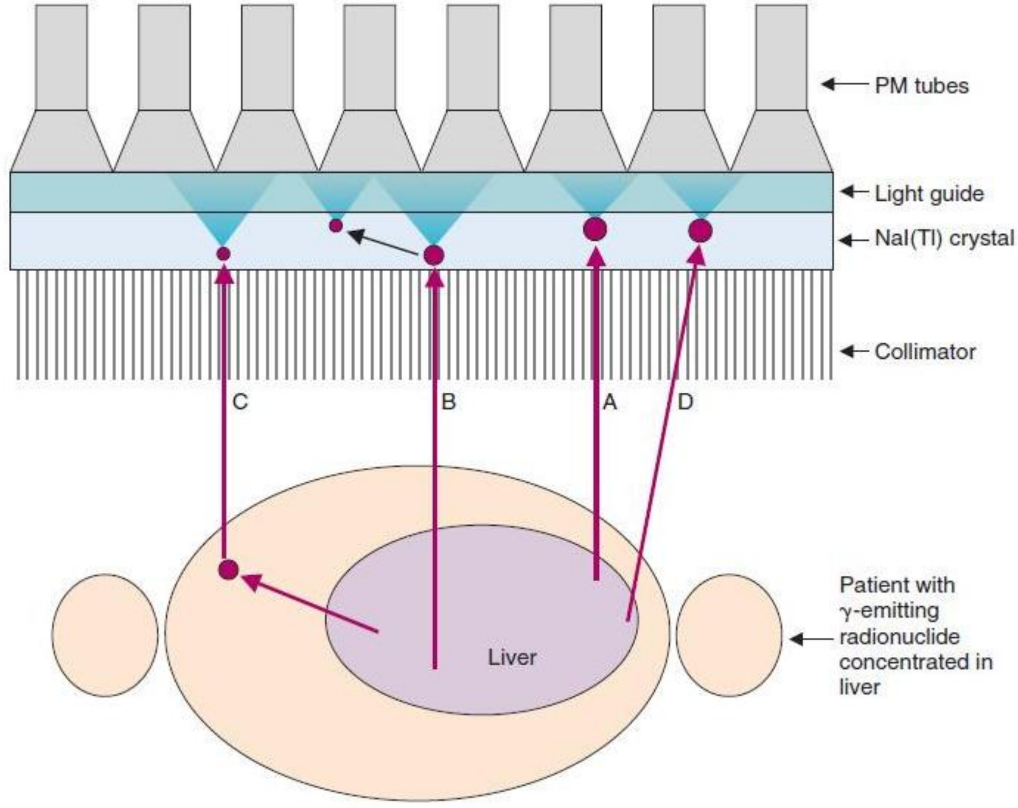

A) Valid event (useful for correct localization on the imaged region)
B) Scatter on the crystal
C) Scatter on the patient
D) Septal penetration

Incorrect source localization

Event localization on the crystal surface

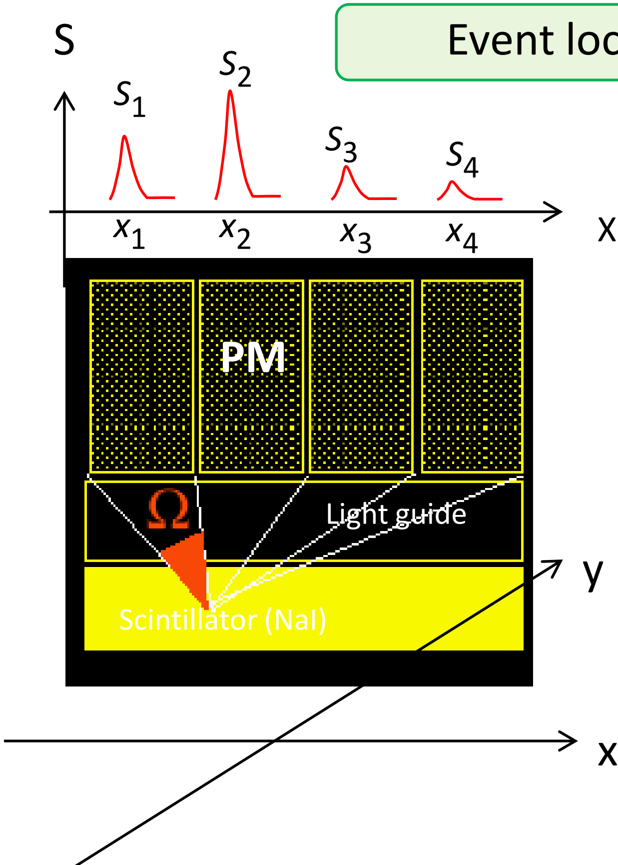

Centroid of the PM response

$$x = \frac{\sum_{i=1}^{n} S_i x_i}{\sum_{i=1}^{n} S_i} \qquad y = \frac{\sum_{i=1}^{n} S_i y_i}{\sum_{i=1}^{n} S_i}$$

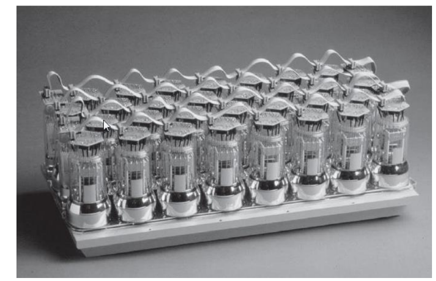

Software positioning also account for non-linearity
In PM response

Pulse height analysis and energy determination

Discriminate gamma events
Scattered photons

Threshold level on signal height
→ Acceptance energy window
(photoelectric peak)

No scatter (or low scatter) is accepted
for image formation

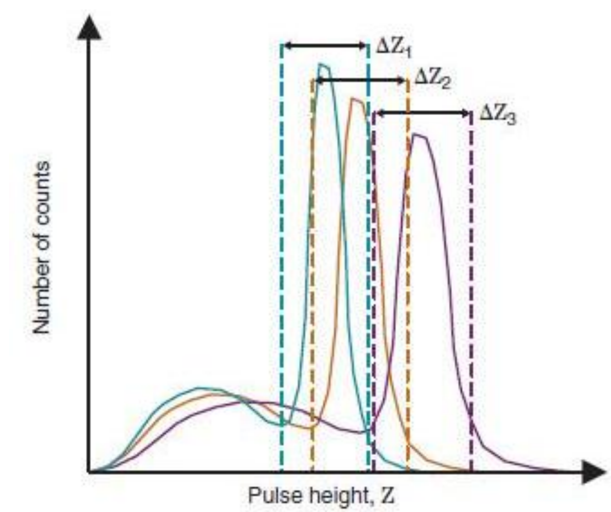

Gamma camera: Performances

Intrinsic spatial resolution (detector)
→(4mm)

- ➢ Impinging gamma energy
- ➢ Crystal thickness

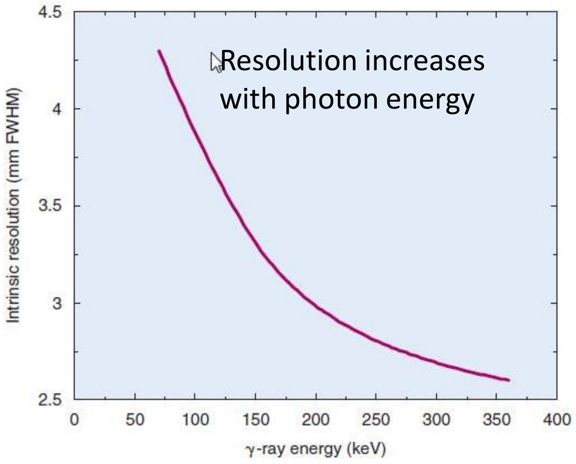

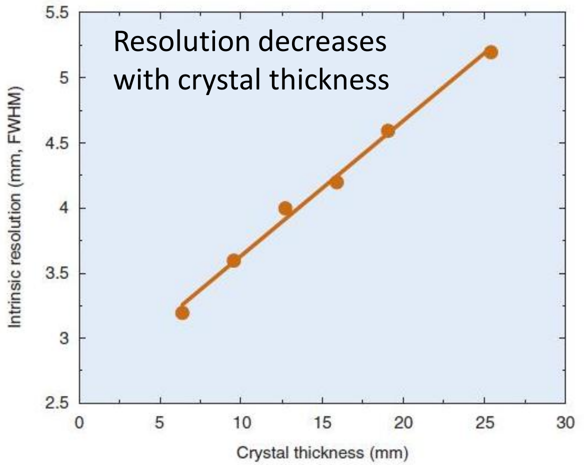

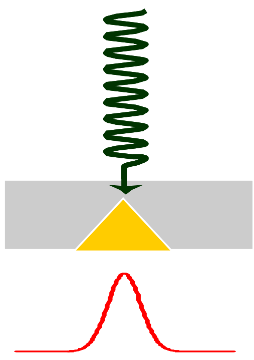

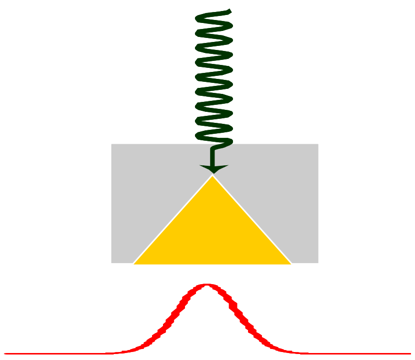

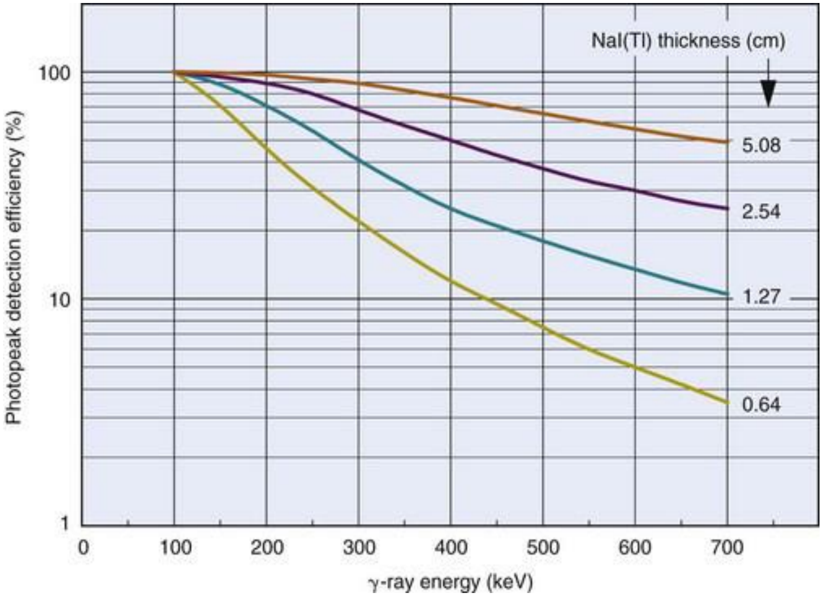

Gamma Camera: collimator resolution

Collimator resolution (parallel-hole)
~10 mm

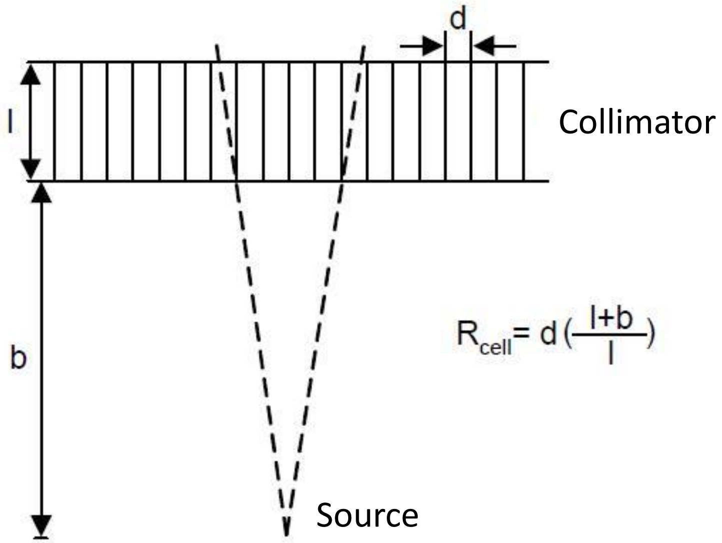

$$R_{cell} = d\left(\frac{l+b}{l}\right)$$

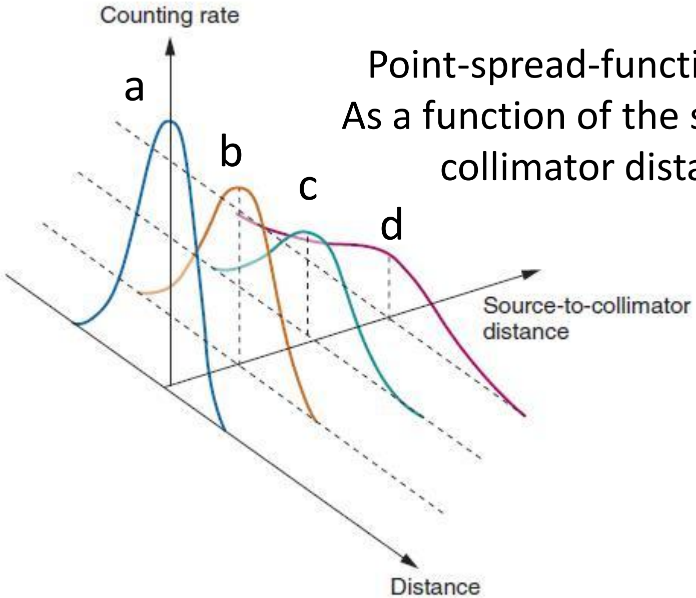

Point-spread-function (PSF)
As a function of the source-to-collimator distance

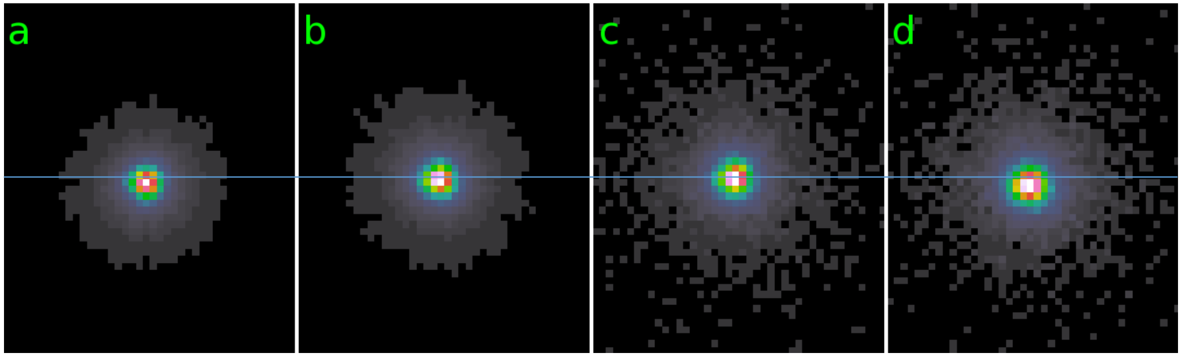

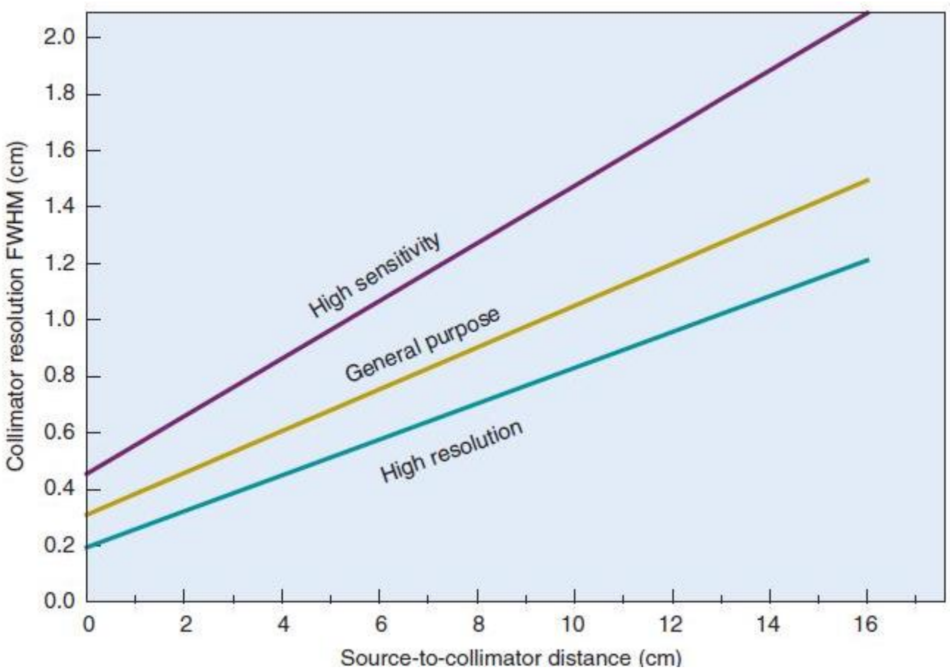

Gamma camera total resolution

R_I = 3.5 mm

R_{coll} = 10 mm

Compute the total resolution !!!!

$$R_{tot} = \sqrt{R_I^2 + R_{coll}^2}$$

$$= \sqrt{3.5^2 + 10^2} = 10.7mm$$

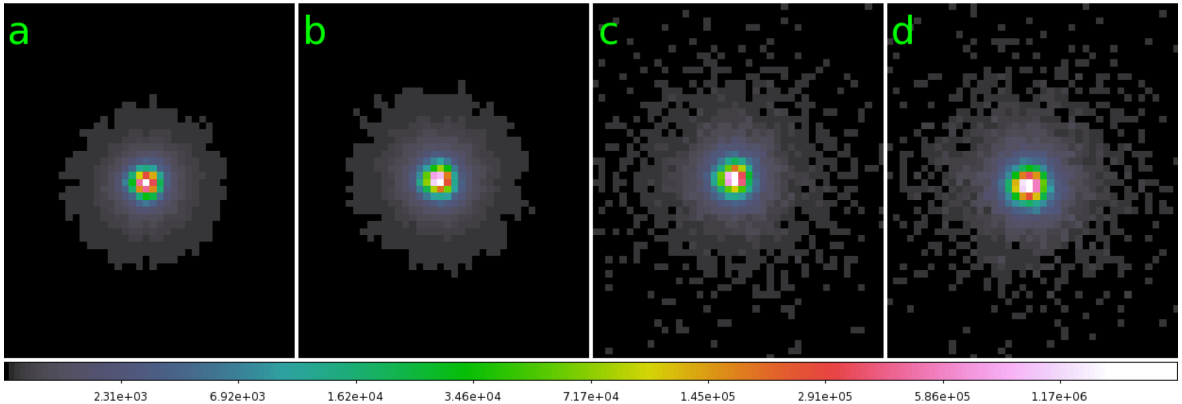

Gamma camera Sensitivity

Collimator Efficiency

$$S_{coll} = \frac{\Omega}{4\pi}\frac{A_{holes}}{A_{crystal}} = \frac{\pi\left(\frac{d}{2}\right)^2 \Big/ l^2}{4\pi}\frac{A_{holes}}{A_{crystal}}$$

Ω: solid angle subtended by the collimator hole from the source
d : collimator hole diameter
l : collimator length (septa length)

Total Efficiency

$$S_{tot} = \frac{\Omega}{4\pi}\frac{A_{holes}}{A_{crystal}} \times \left[1 - e^{-\mu d_{crystal}}\right]$$

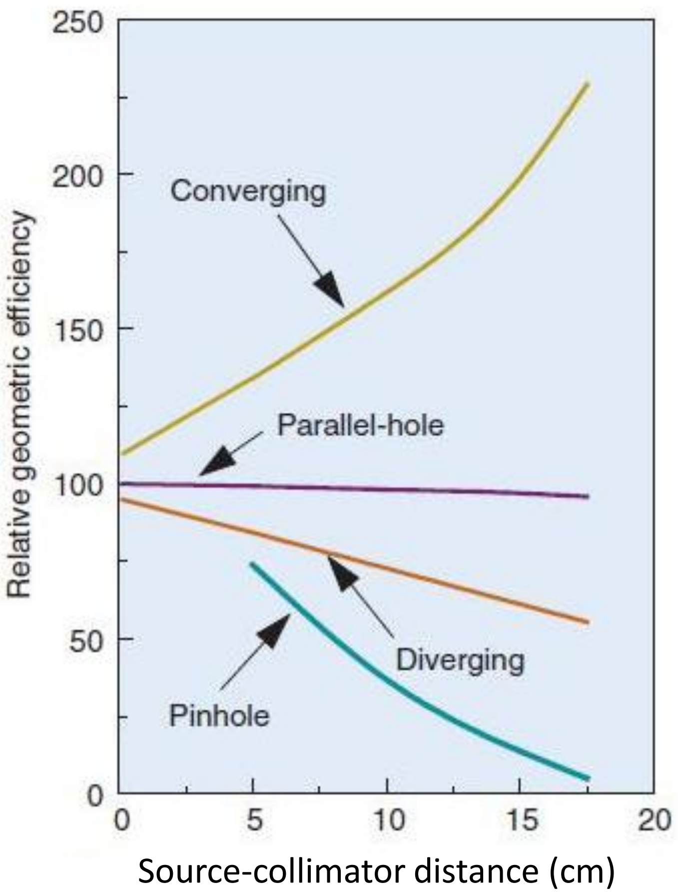

- Ex-1 Determine the sensitivity of a parallel-hole collimator characterized by:

l = 3 cm
d = 2.5 mm
(A_{holes} /$A_{crystal}$) =0.8

$$S_{coll} = \frac{\Omega}{4\pi}\frac{A_{holes}}{A_{crystal}} = \frac{\pi\left(\frac{d}{2}\right)^2 \Big/ l^2}{4\pi}\frac{A_{holes}}{A_{crystal}}$$

= {[(2.5/2)^2]/(4 × 30^2)} × 0.8
= 3.47E-04

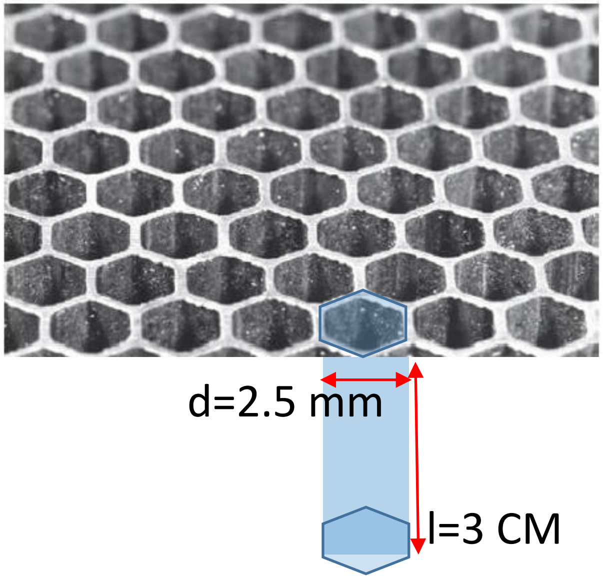

➢EX-2 Determine the global system sensitivity for a camera system having the same collimator, NaI crystal thickness of 7 mm measuring ^{99m}Tc gamma rays.

$$S_{tot} = \frac{\Omega}{4\pi} \frac{A_{holes}}{A_{crystal}} \times \left[1 - e^{-\mu d_{crystal}}\right]$$

μ(NaI, 140 keV) = 3.04 cm^{-1}

S_{coll} = {[(2.5/2)^2]/(4 × 30^2)} × 0.8
= 3.47E-04

S_{tot} = S_{coll} × [1-exp(-3.04 cm^{-1} × 0.7cm)]

= 3.47E-04 × 0.88 = 3.05E-04

Gamma camera Sensitivity

Collimator Efficiency

$$S_{coll} = \frac{\Omega}{4\pi}\frac{A_{holes}}{A_{crystal}} = \frac{\pi\left(\frac{d}{2}\right)^2 \Big/ l^2}{4\pi}\frac{A_{holes}}{A_{crystal}}$$

Ω: solid angle subtended by the collimator hole from the source
d : collimator hole diameter
l : collimator length (septa length)

Total Efficiency

$$S_{tot} = \frac{\Omega}{4\pi}\frac{A_{holes}}{A_{crystal}} \times \left[1 - e^{-\mu d_{crystal}}\right]$$

Source-collimator distance (cm)

Collimator Type	Recommended Max. Energy (keV)	Efficiency, g	Resolution R_{coll} (FWHM at 10 cm)
Low-energy, high-resolution	150	1.84×10^{-4}	7.4 mm
Low-energy, general-purpose	150	2.68×10^{-4}	9.1 mm
Low-energy, high-sensitivity	150	5.74×10^{-4}	13.2 mm
Medium-energy, high-sensitivity	400	1.72×10^{-4}	13.4 mm

The reasons for SPECT…
… Beyond planar imaging

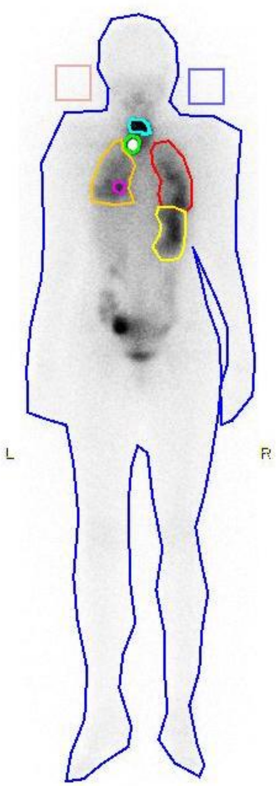

WB1
D+3.

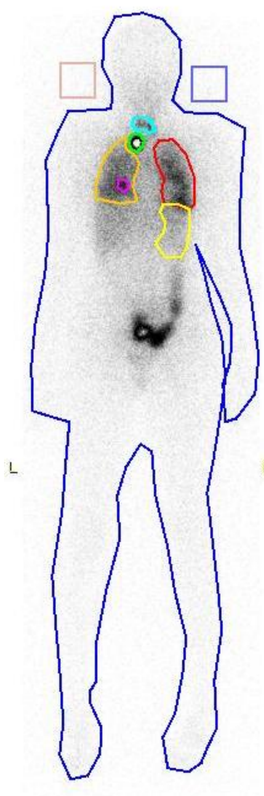

WB2
D+8.

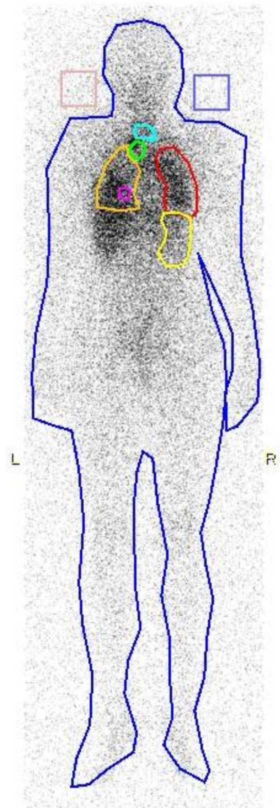

WB3
D+15

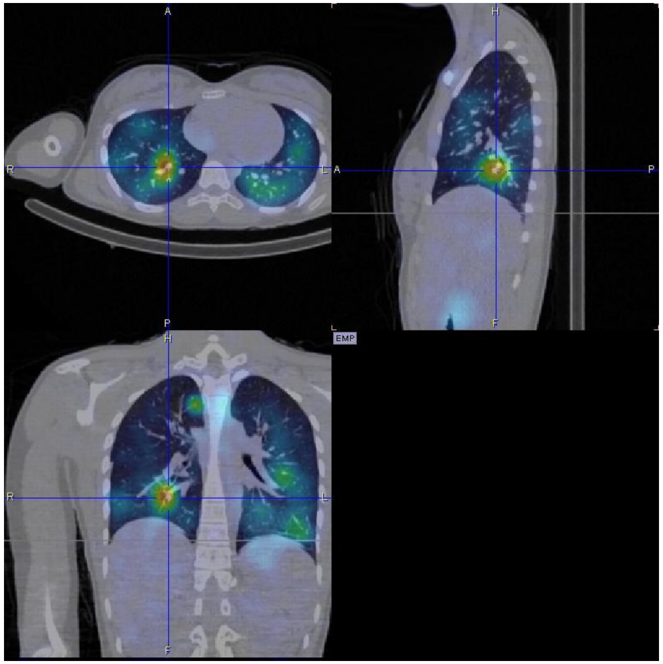

- ➢ Improved emission localization
- ➢ Disentangle signal overlap
- ➢ Pave the way to 3D quantitative imaging

Introduction to tomography in nuclear medicine

Bases of tomography reconstruction in nuclear medicine

Measured projection profile

Detector

Collimator

Imaged object

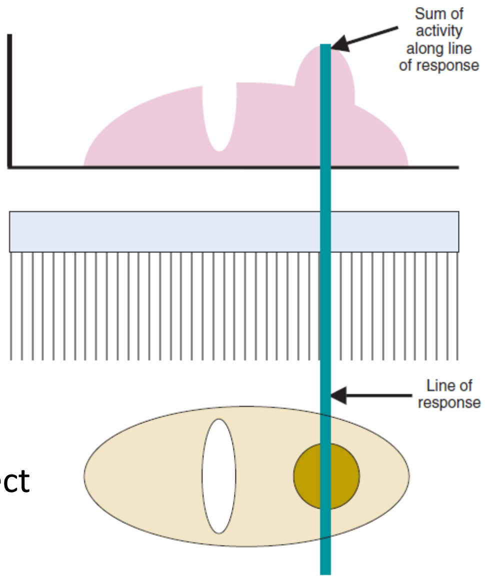

Spatial activity distribution

Projections in a simple 1-D detector case

Signal proportional to the summed activity along the line of response
(assumption of no attenuation and scatter)

Head rotation around the imaged object

Many projections at different angles are obtained

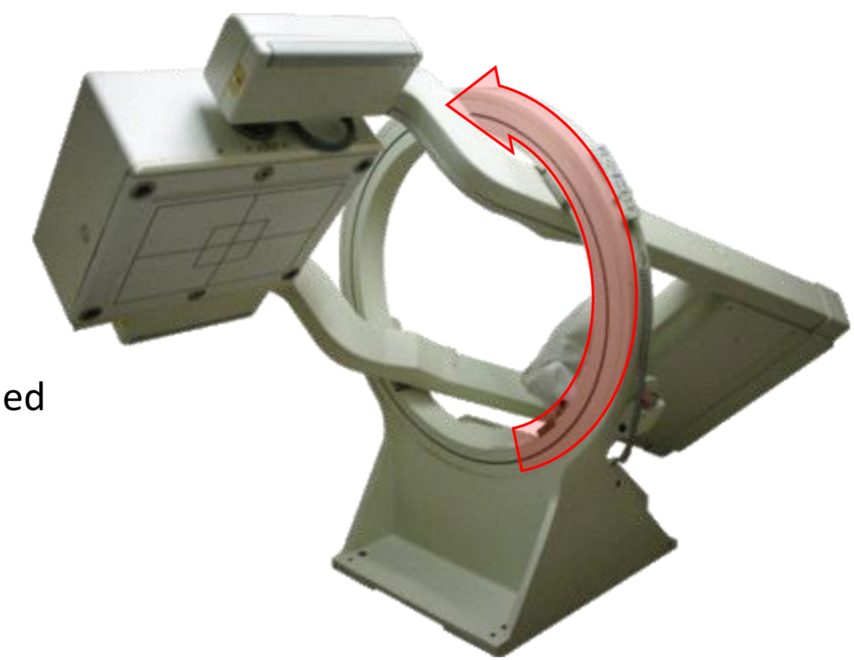

1-D projections of a unknown activity distribution *f(x,y)*

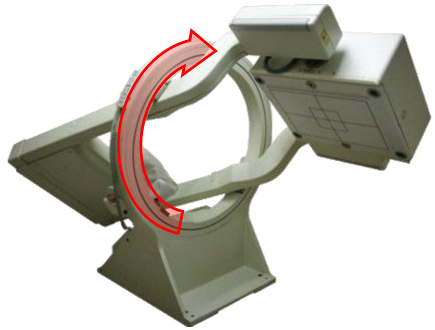

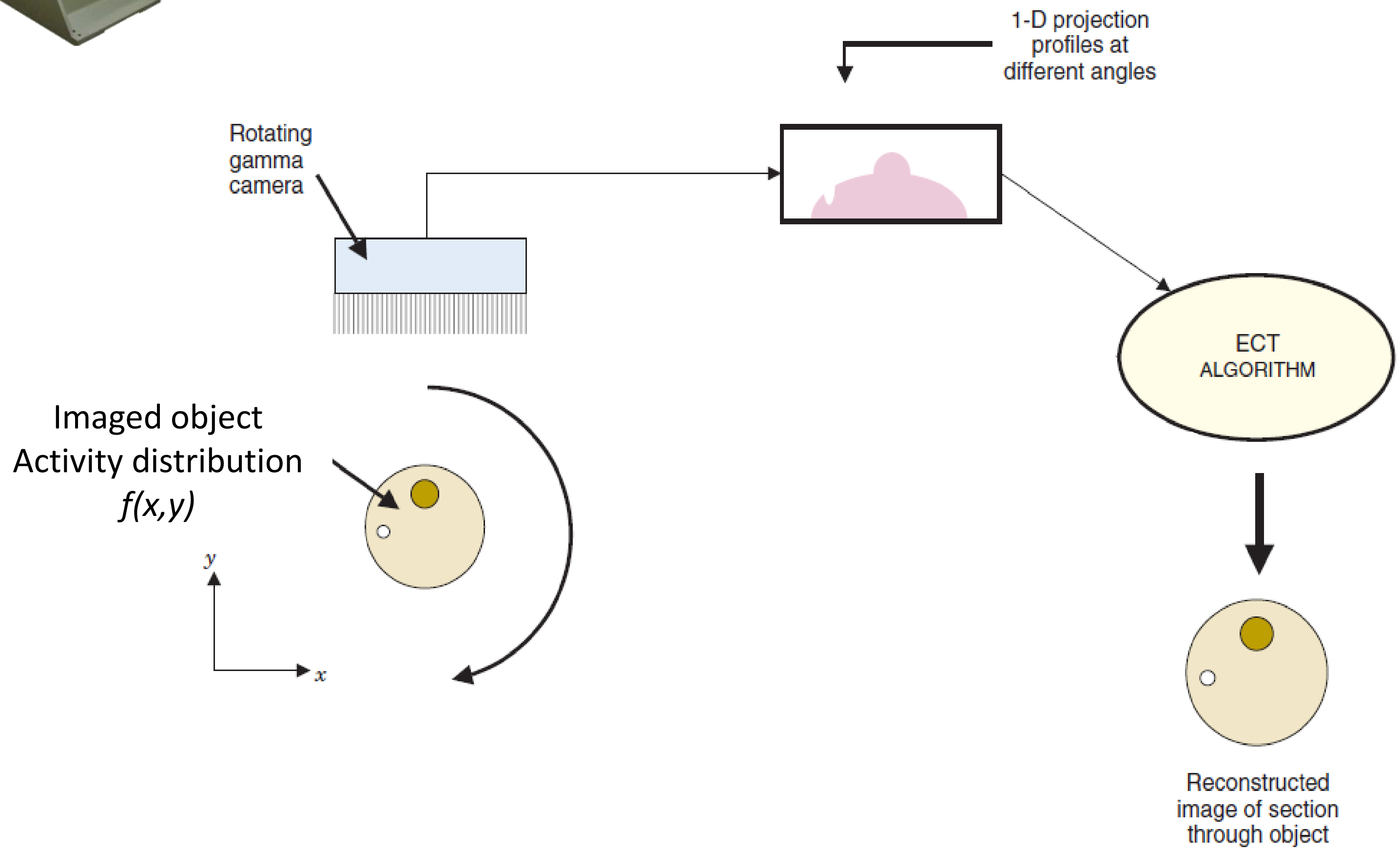

Principle of (forward) projection for one 3×3 slice at angle θ = 0 and θ = 90°

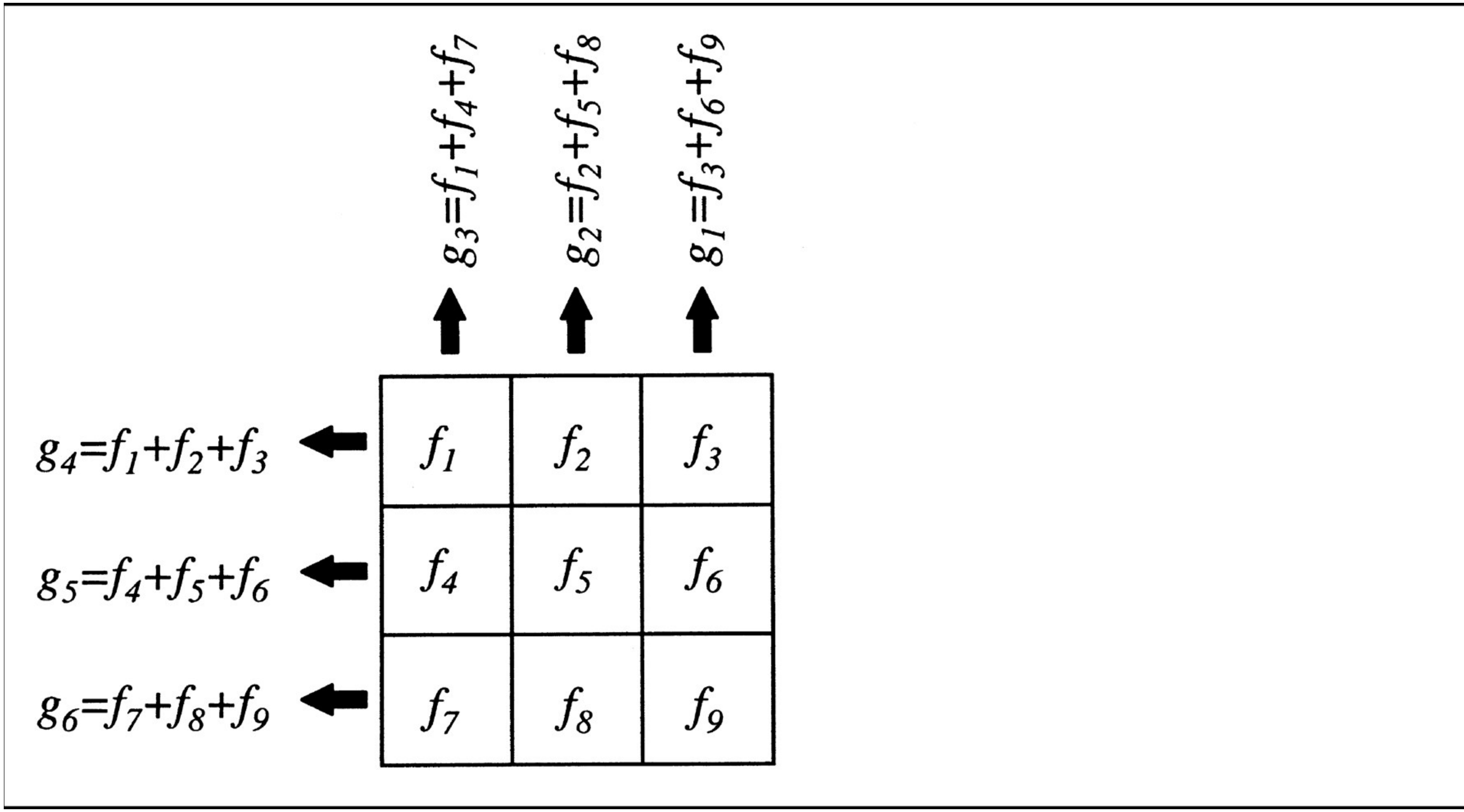

Bruyant et al, JNM, 2002

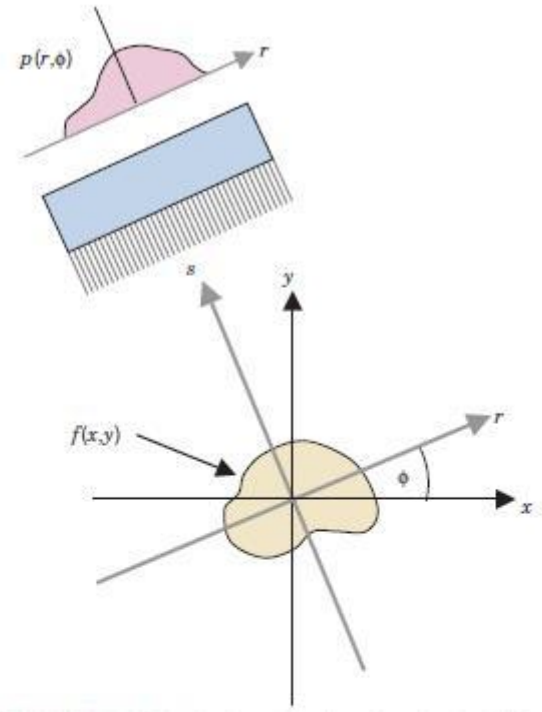

N projections are recorded around the emitting Object (0-360 deg)

N projections p(r,ϕ)

Angular spacing is A_s = 360/N deg

Typically A_s = 3 deg for N = 120 projections
ϕ = (0=360 deg), 3deg, 6deg,…

Dual Head Camera → 60 acquisition steps

15 sec per step →15 minutes image acquisition

Projection data are arranged in
(r,ϕ) : coordinate frame stationary
with respect to the detector-camera frame

(x,y) → (r,ϕ)

$$r = x\cos\varphi + y\sin\varphi$$

$$s = y\cos\varphi - x\sin\varphi$$

Base for SINOGRAM representation

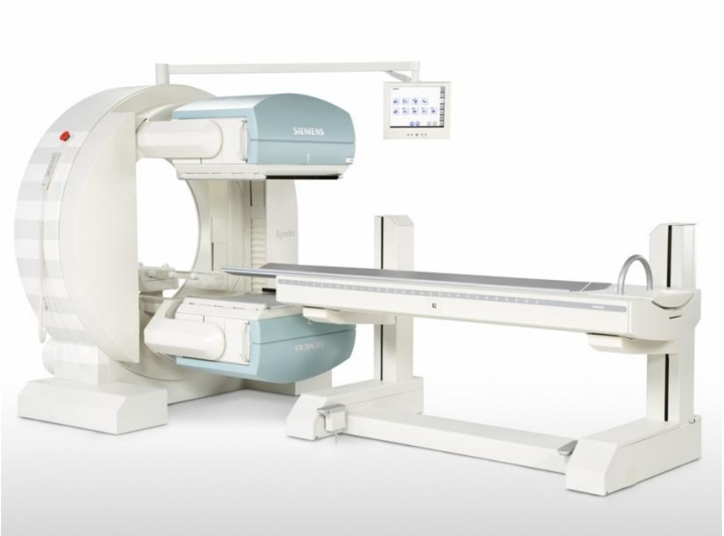

N projections p(r,ϕ) ⟺ N angular samples ⟺ N sinogram lines in the (r,ϕ) space

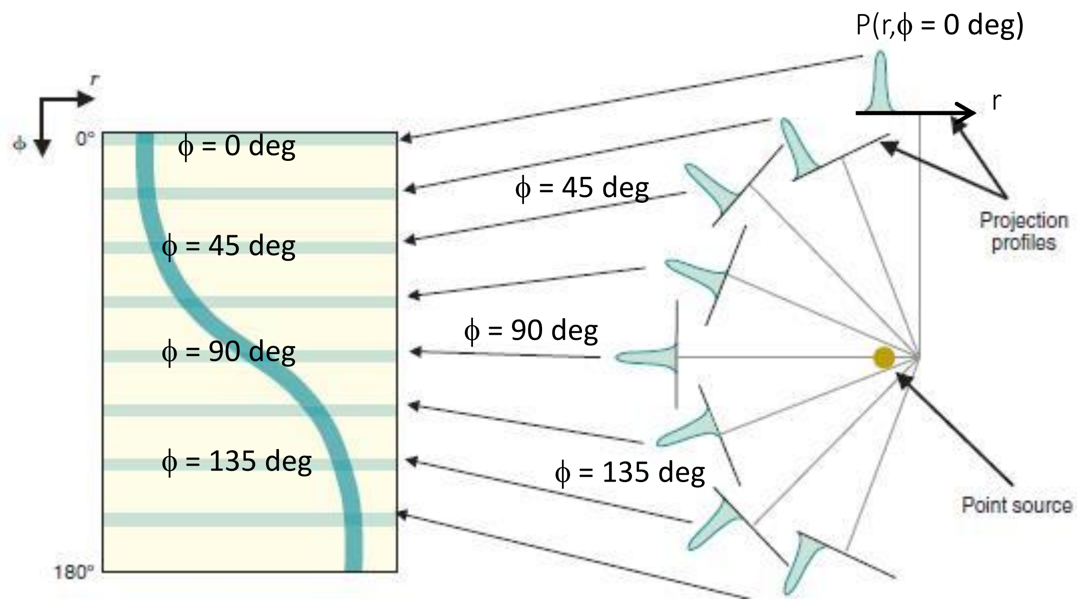

1-D Projection data are arranged in a 2D (r,ϕ) **SINOGRAM representation**

Each row (ϕ) in the sinogram displays the intensity profile measured in the corresponding projection

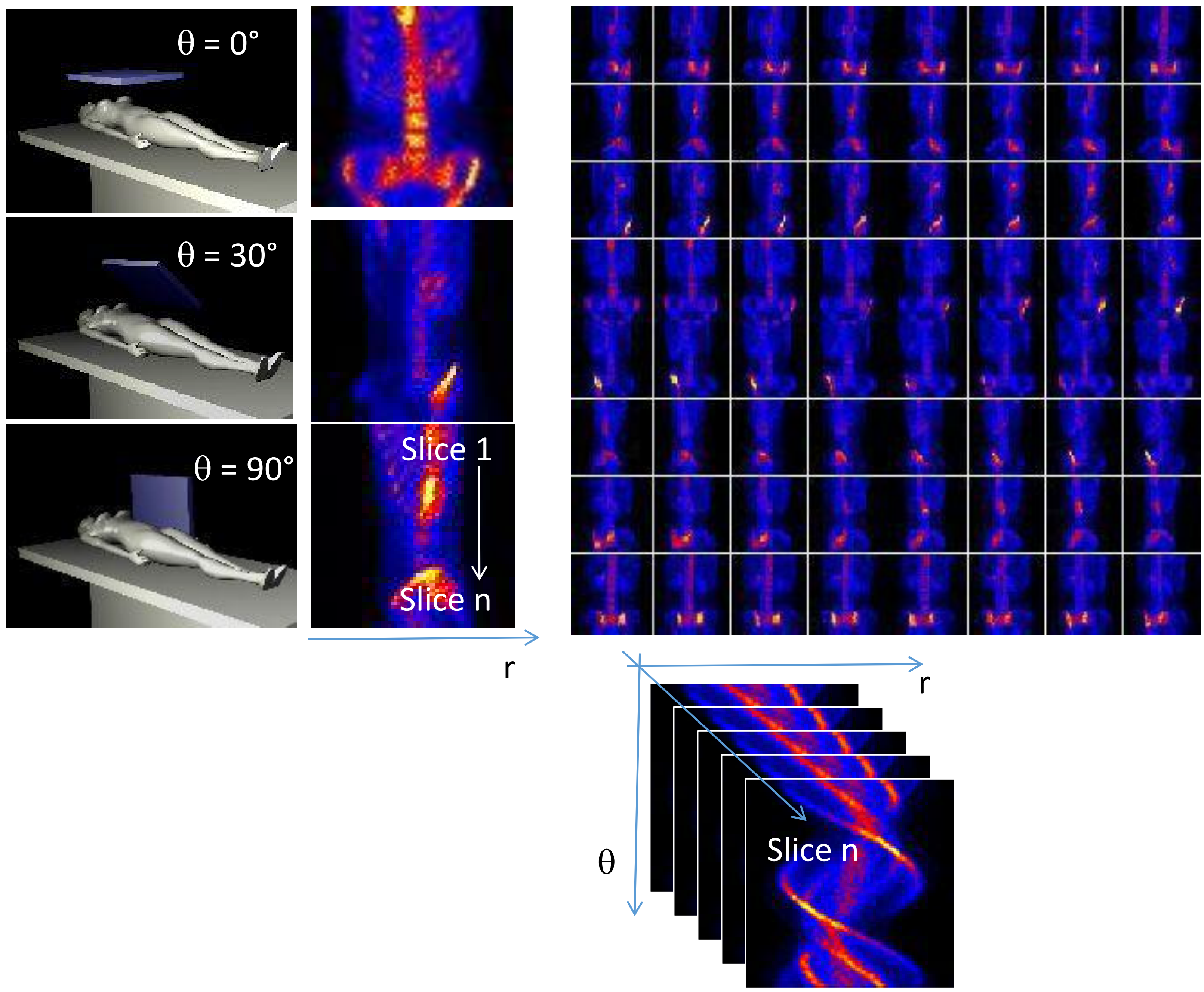

θ = 0°
θ = 30°
θ = 90°
Slice 1
Slice n
r
r
θ
Slice n

What we have: a discrete number of measured projections $P(r,\phi)$
Arranged in a sinogram

What we want: Recover the unknown activity distribution $(f(x,y))$

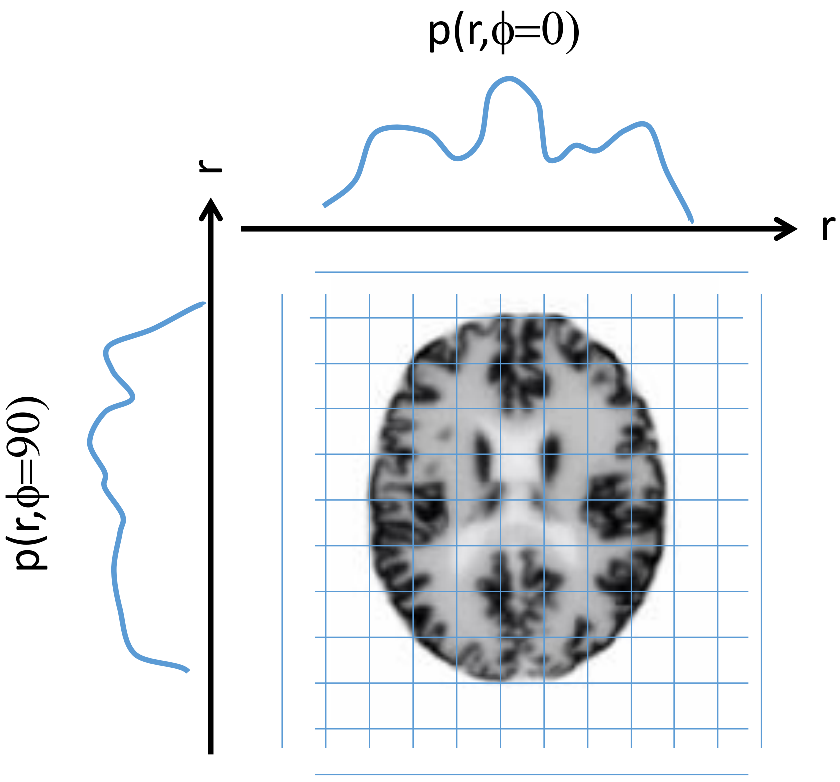

The reconstructed activity distribution $f'(x,y)$ in a 2D plane of discrete pixels.

Matrix dimension in SPECT is typically 128 x 128

Simple Back Projection

The unknown activity distribution is reconstructed by distributing the measured Intensity back across the (pixelized) construction plane

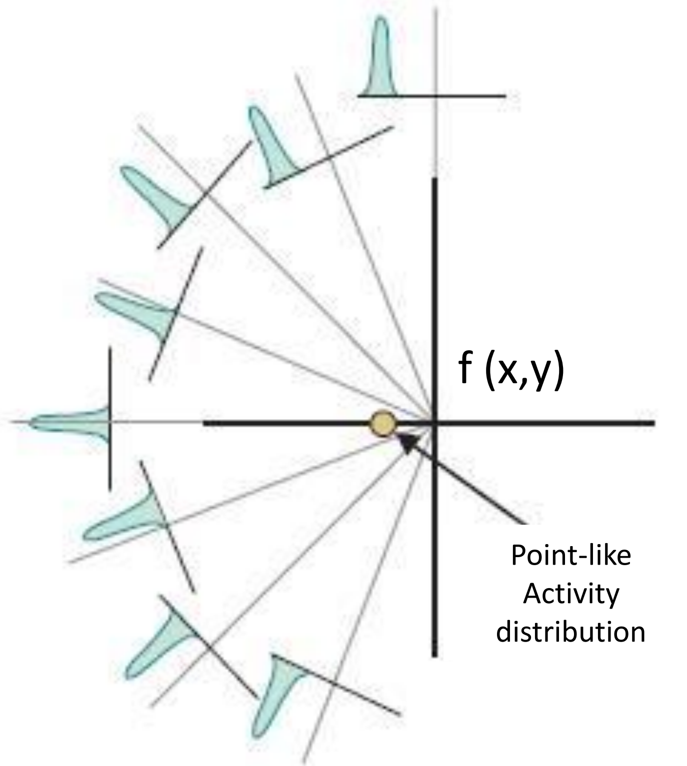

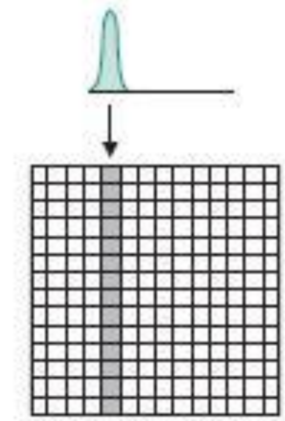

Backprojection of intensity profile at ϕ = 0 deg across the reconstruction plane

2 projection angles ϕ = 0, 90 deg | 8 projection angles | 256 angles

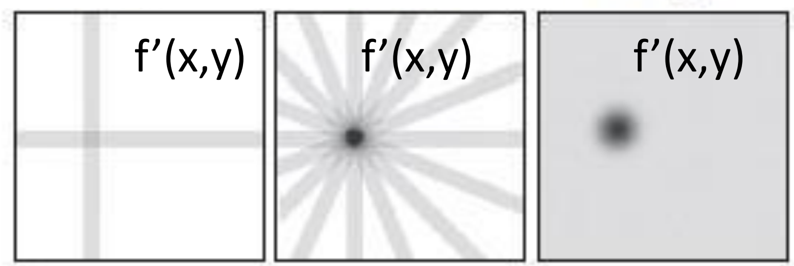

$$f'(x,y) = \frac{1}{N}\sum_{i=1}^{N} p(x\cos\varphi_i + y\sin\varphi_i, \varphi_i)$$

Simple Backprojection results in a blurred reconstructed image

$$f'(x,y) = f(x,y) * (1/r)$$

1/r blurring
Low image contrast

Simple Backprojection of an activity distribution in phantom

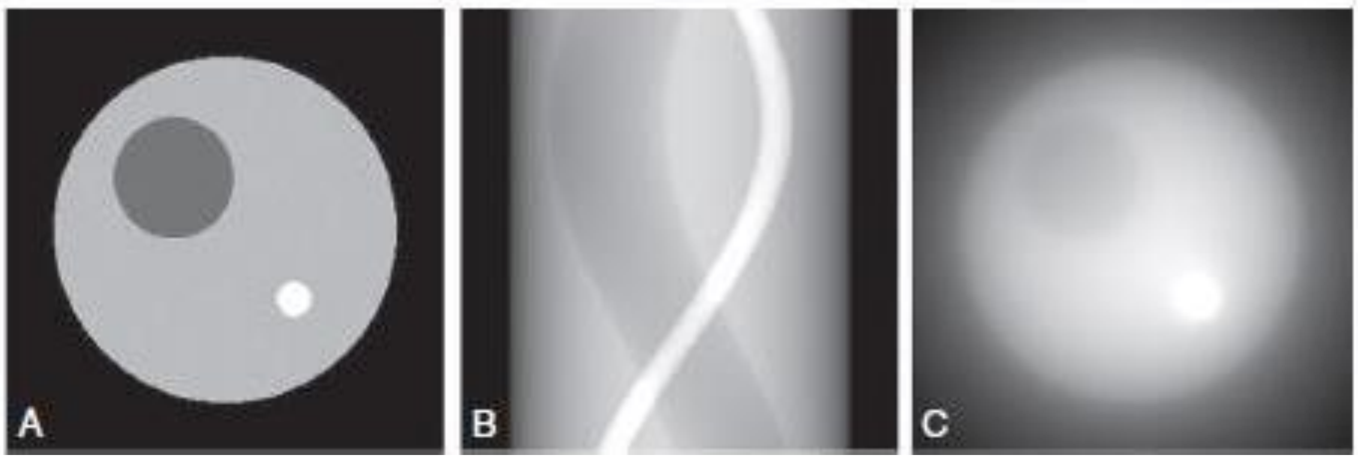

A: Simulated phantom activity distribution
B: Sinogram (256 projection angles)
C: Simple Backprojection Reconstruction

1/r blurring — Degradation of sharper details (edges)

Degradation of contrast

Simple Backprojection of an activity distribution in brain

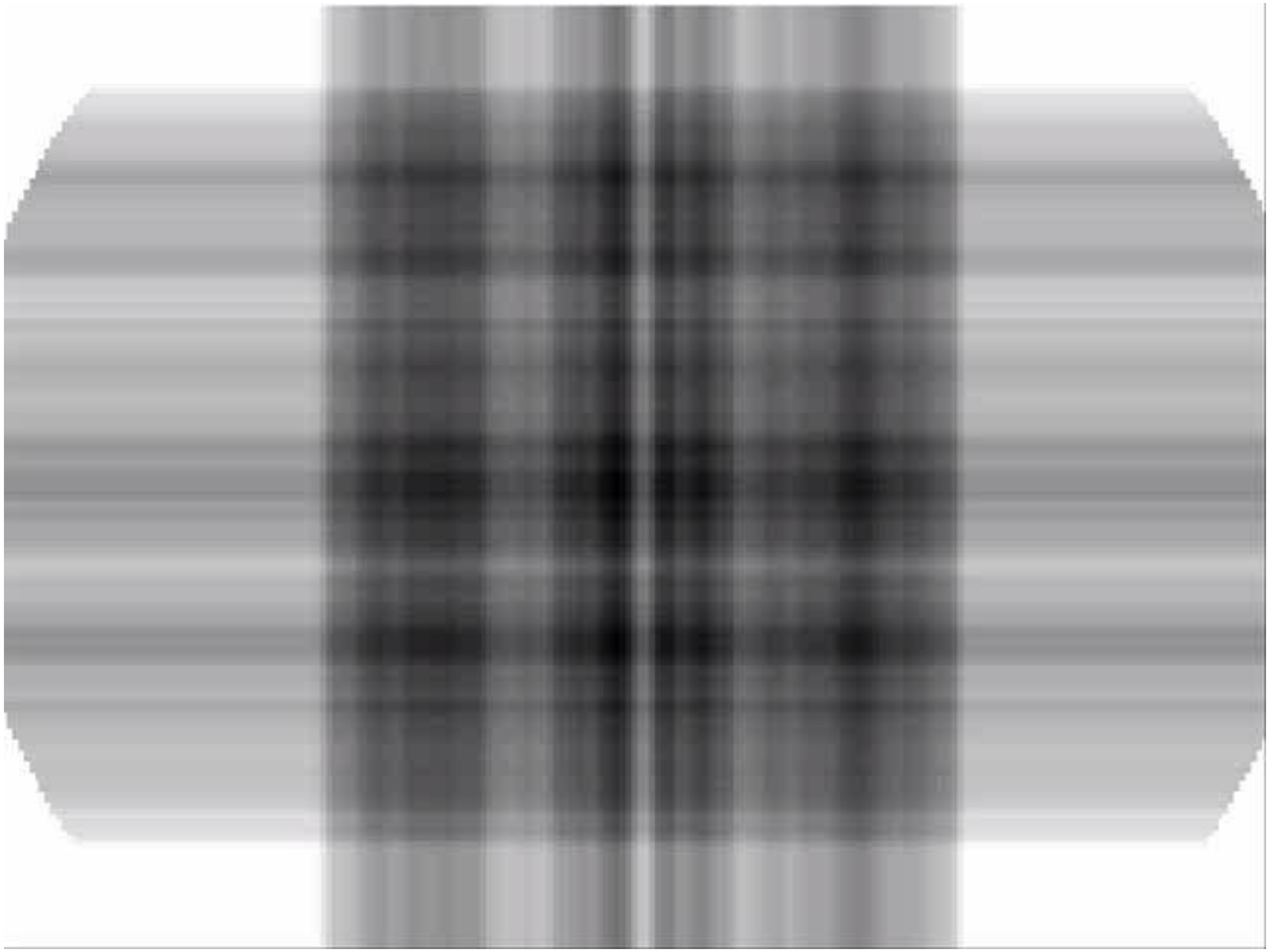

Simple Backprojection results in a blurred reconstructed image

Direct Fourier Transform reconstruction

Avoid 1/r blurring

Image space (object space)

1D $f(x)$

2D $f(x,y)$

$$F^{-1}\left[F\left(k_x,k_y\right)\ \right] = f(x,y)$$

Frequency space
k-space

$$F(k) = FT(f(x))$$

$$F\left(k_x,k_y\right) = FT(f(x,y))$$

Projection slice theorem

$$FT[p(r,\varphi)] = P(k,\varphi)$$

Image space
(object space)

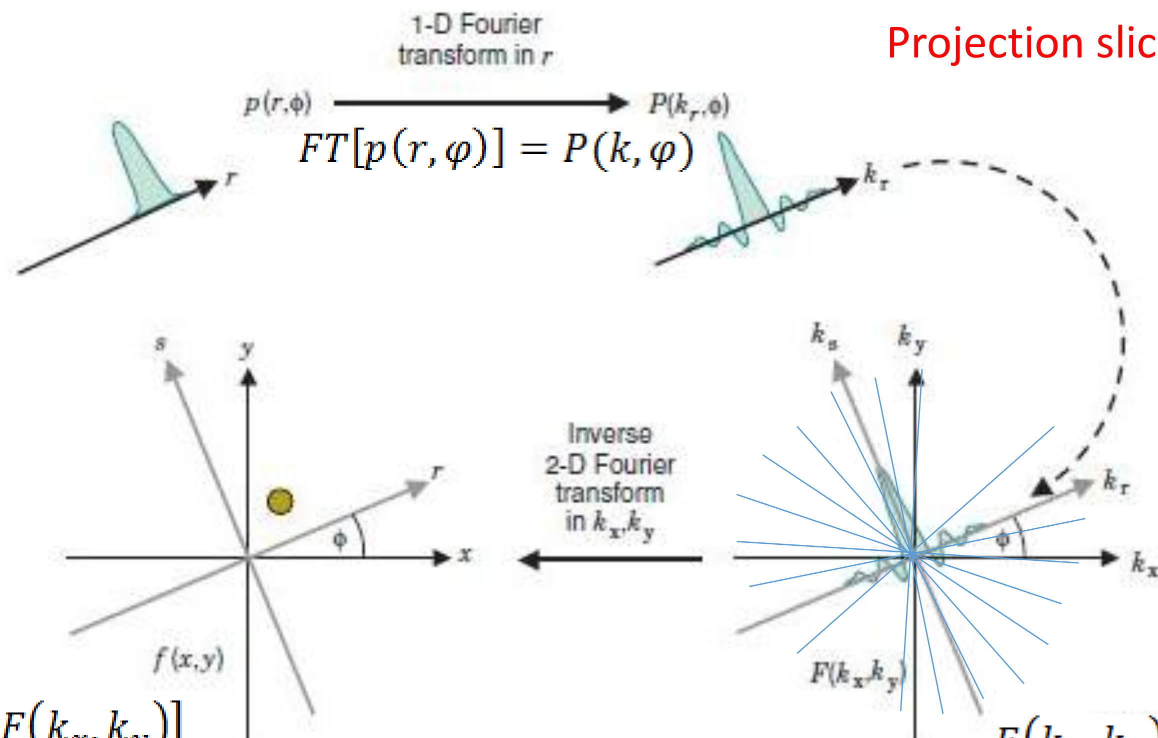

Frequency space
k-space

$$f(x,y) = F^{-1}\left[F\left(k_x,k_y\right)\right]$$

$$F\left(k_x,k_y\right) = FT(f(x,y))$$

Direct Fourier Transform reconstruction

Still affected by 1/r noise (low spatial frequency noise)

Filtered Backprojections (FBP)

1) $FT[p(r,\varphi)] = P(k,\varphi)$

2) $P'(k_r,\varphi) = |k_r| P(k_r,\varphi)$

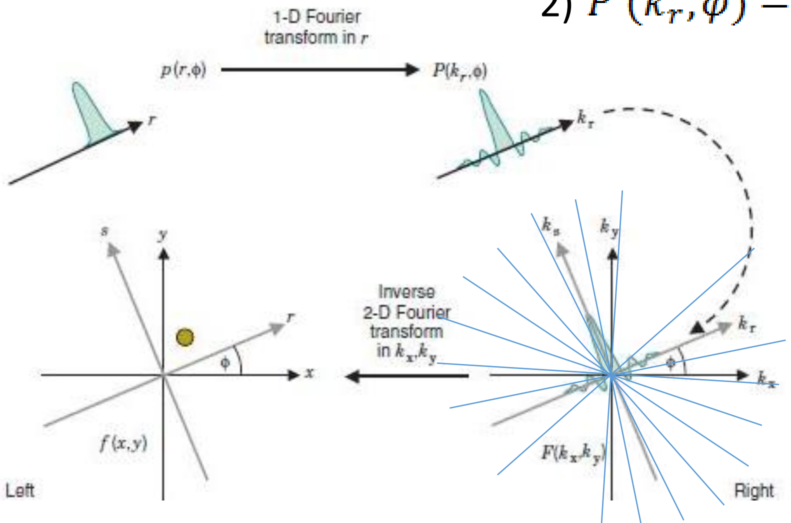

3) $p'(r,\varphi) = FT^{-1}[P'(k_r,\varphi)]$
$= FT^{-1}[|k_r| P(k_r,\varphi)]$

1) Projections are Fourier transformed in k-space

2) Filtering in k-space

3) Inverse Fourier Tranform
to obtain filtered projection in sinogram space (r,ϕ)

4) Backporjection in object space (x,y)

$$f'(x,y) = \frac{1}{N}\sum_{i=1}^{N} p'(x\cos\varphi_i + y\sin\varphi_i, \varphi_i)$$

$H(k_r) = |k_r|$

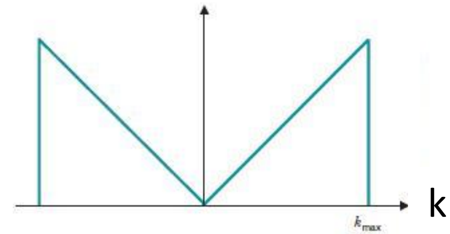

Filtering in k-space precedes
Backprojection into object space

Ramp filter
- Low frequency damping
- High frequency amplifications

1/r blurring is eliminated
But high frequency noise is generated

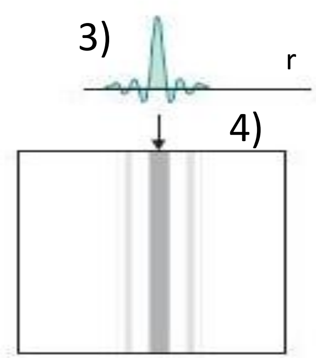

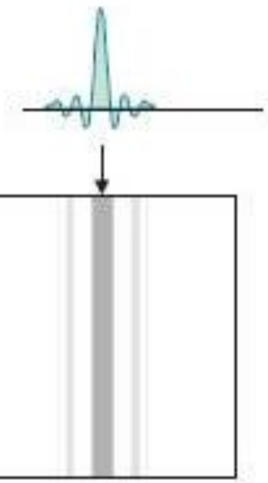

4) Backprojection of filtered profile at ϕ = 0 deg across the reconstruction plane

$$\text{Ramp: } H(k) = |k|$$

$$\text{Shepp–Logan: } H(k) = \frac{2k_{\text{cut-off}}}{\pi} \sin \frac{|k|\pi}{2k_{\text{cut-off}}}$$

$$\text{Hann: } H(k) = 0.5\,|k|\left[1+\cos\frac{\pi k}{k_{\text{cut-off}}}\right]$$

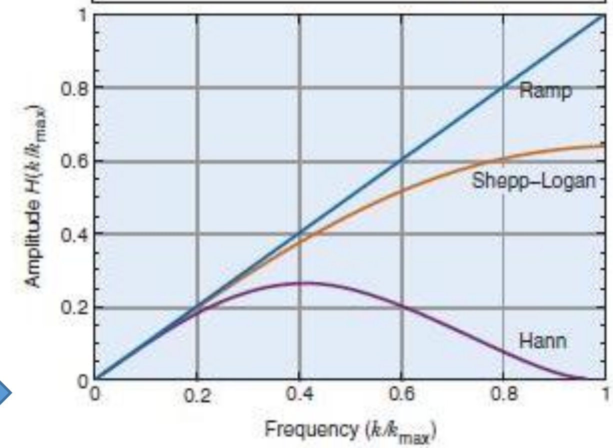

Filtered backprojection at

2 angles 4 angles 256 angles

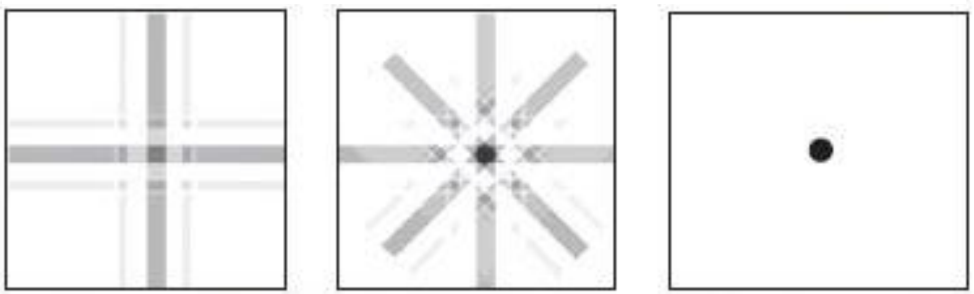

Ramp filter
- Low frequency damping
- High frequency amplifications

High frequency noise induction

SNR degradation

Fitered Backprojection (FBP) of an activity distribution in brain

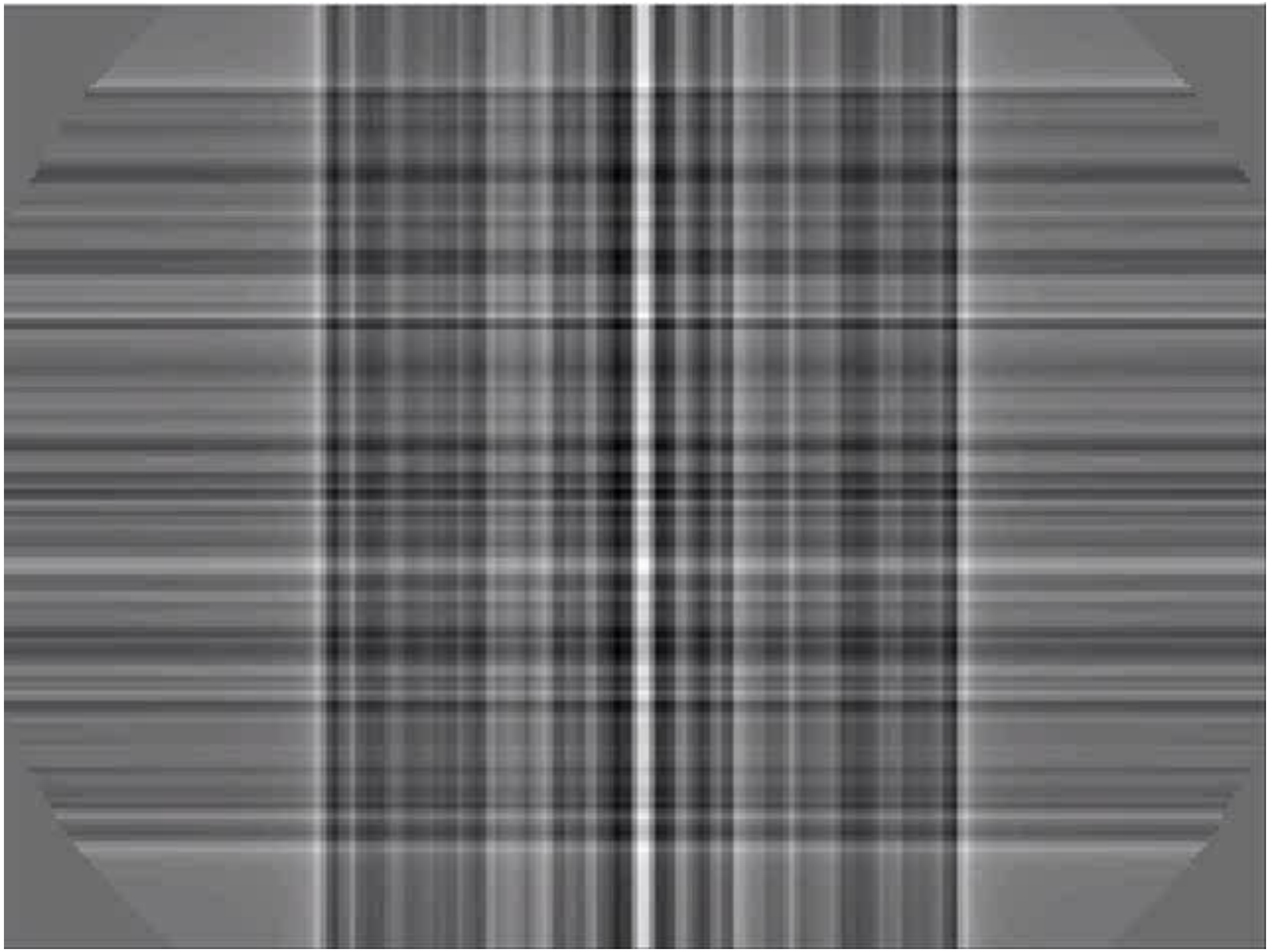

If noiseless projections are available
And virtually infinite angles views are available

Quantitative true activity distribution reconstruction

Summary of FBP characteristics

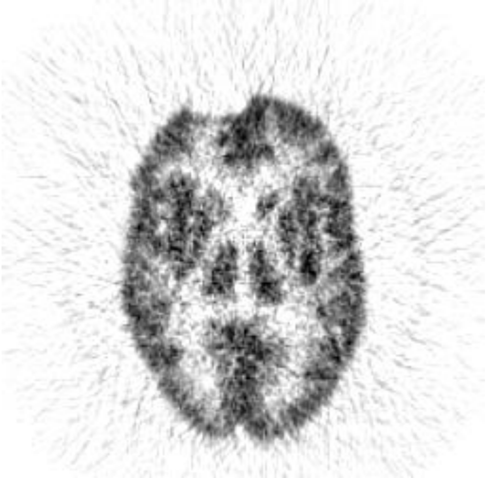

- **Assets:**
  - Accurate (quantitative) if noise-free measurements and completely sampled data
  - Fast and easy to implement

- **Limitations:**
  - Still noisy (steak artifacts)
  - No natural way to implement Corrections:
    - Spatial resolution
    - Scattering
    - attenuation

Iterative reconstruction techniques

Iterative Reconstruction algorithm

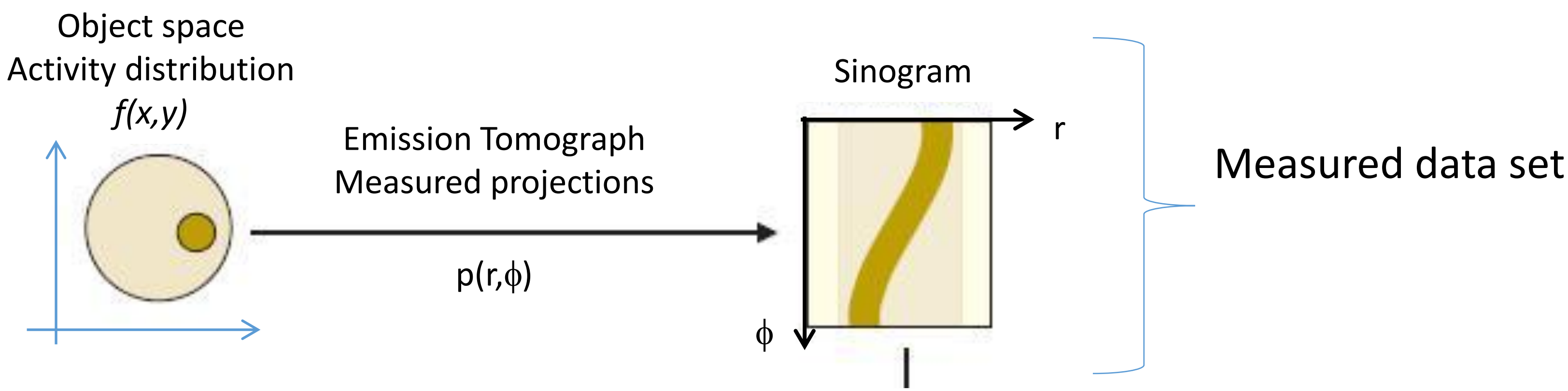

Iterative reconstruction

More computationally demanding
Than FPB

Now become standard in clinic

True activity distribution *f(x,y)*
is estimated by successive
approximations *f'(x,y)*

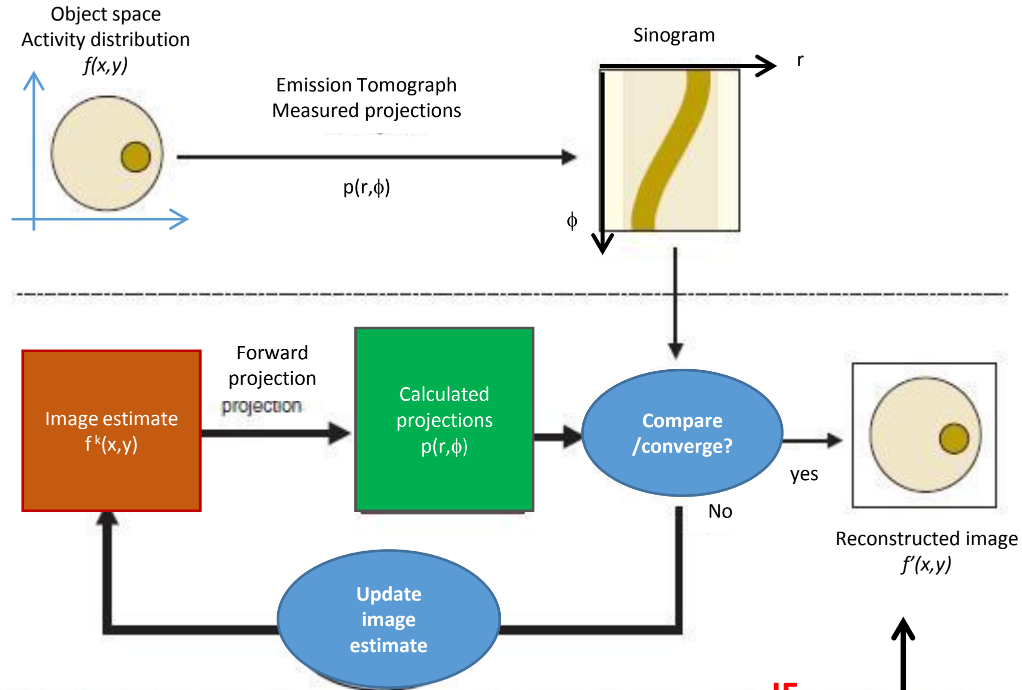

1) Start with a very simple initial
image estimation
- ex.Unifrom activity distribution in the FOV

↓

2) Computed (forward) projections
form $f^k(x,y)$ estimate

↓

3) Computed Sinogram is compared with
Measured sinogram

↓

4) Compute correction factors → 5-1) Refresh the image estimate

If no convergence

IF Convergence

Example of Iterative Reconstruction

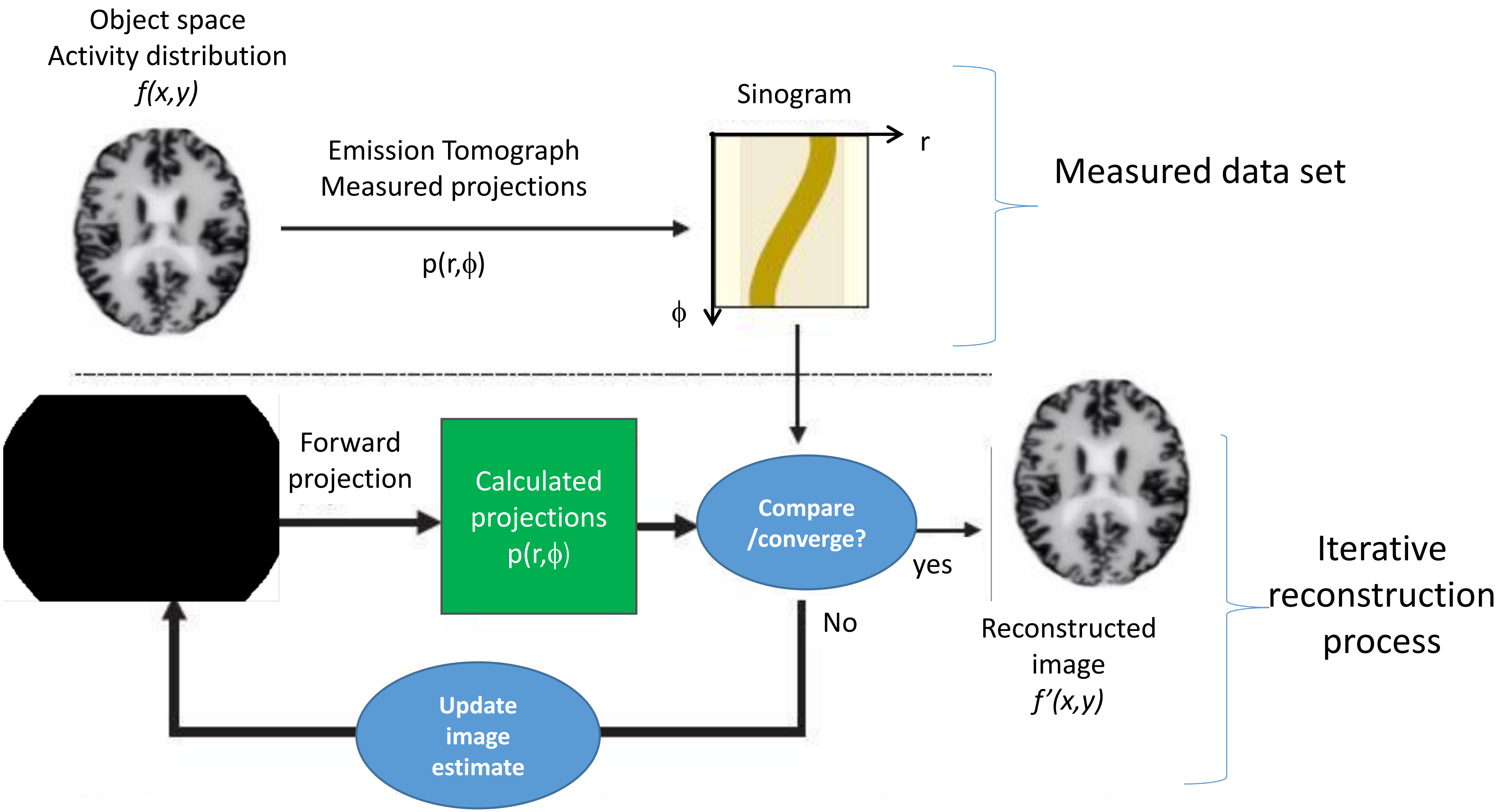

Animations from:
Floris HP van Velden, PhD
EANM Milan 2012

Iterative reconstruction

Key points:

Expectation maximization cost function

(convergence criterion)

Method to upgrade the image estimate

Account for:

- *Detector and collimator response,*
- *finite spatial resolution*
- *Attenuation*
- *Scattering*

Quantitative more accurate than FBP

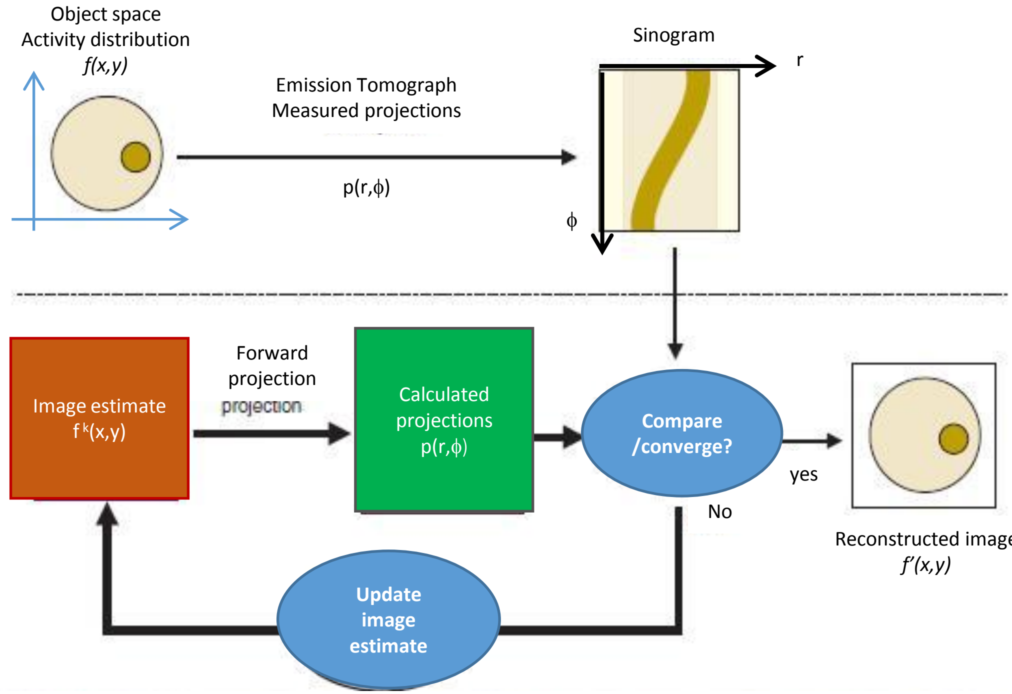

All image pixels (i) have a finite probability ($M_{i,j}$) to contribute to signal intensity into projection data (p_j)

$$p_j = \sum_{i=1}^{n} M_{i,j} f_i$$

$$f_i^{k+1} = \frac{f_i^k}{\sum_{j=1}^{m} M_{i,j}} \times \sum_{j=1}^{m} M_{i,j} \frac{p_j}{\sum_{i'=1}^{n} M_{i',j} f_{i'}^k}$$

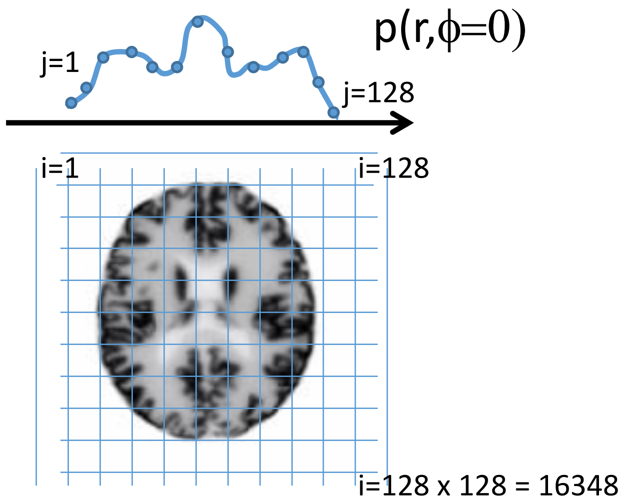

If 120 angular projections → 120 x 128 = 15360 projection data → M : (16348 x 15360)

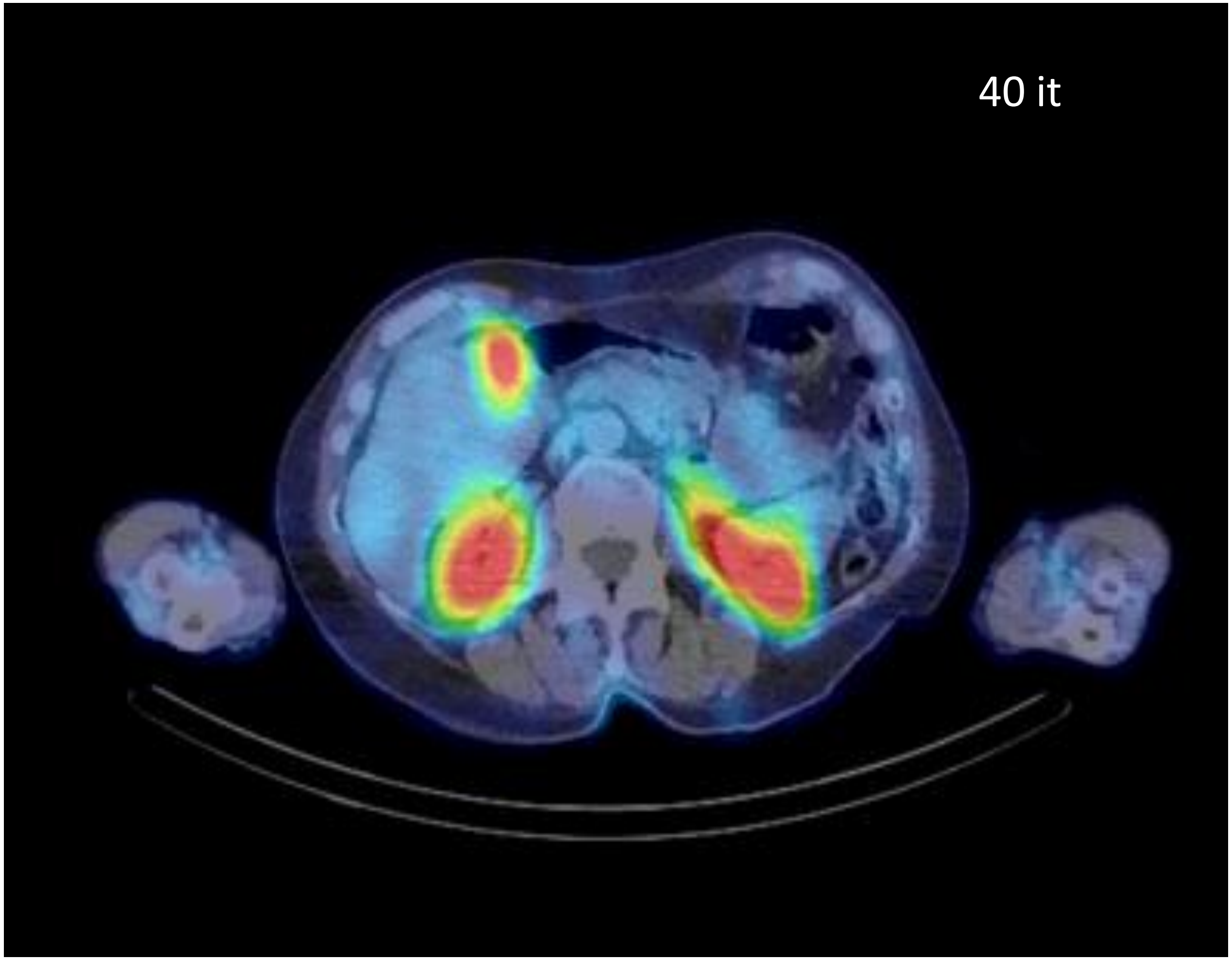
40 it

Single Photon Emission Computer Thomography: SPECT

Single Photon Emission Computer Thomography: SPECT

SPECT systems are based on Gamma Camera technology

Single head

Double head

Triple head

Acquisition: 2D array of 1D-projections
→ 2D planar image

http://meditronics.wordpress.com/spect/

Tomographic reconstruction

2D axial slices
stacked in a 3D array
(3D volume image)

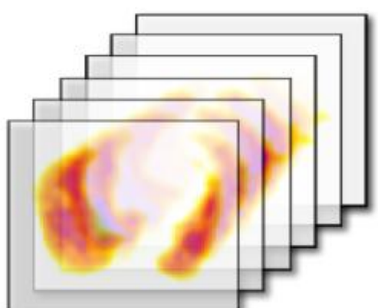

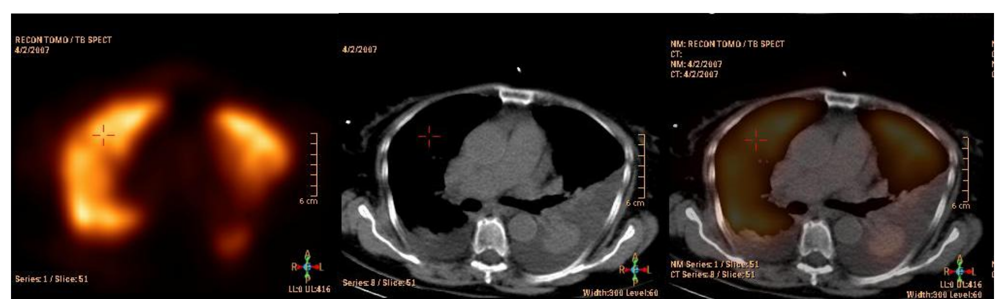

More detection head → **increased detection sensitivity**
→ Reduced acquisition time

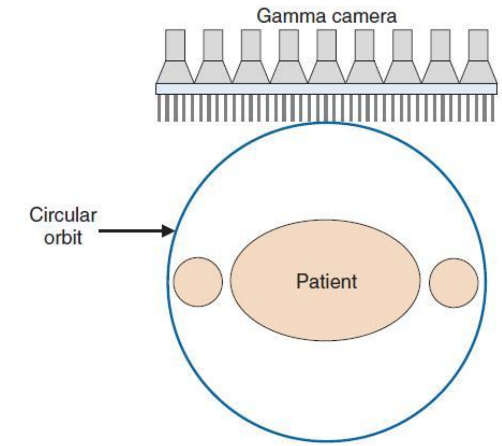

Acquisition orbit
→as close as possible to the Patient contour
→ minimize resolution degradation with distance

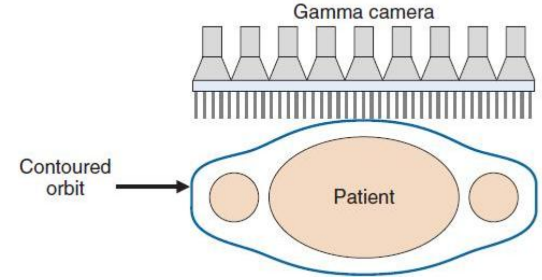

Automatic patient detection systems

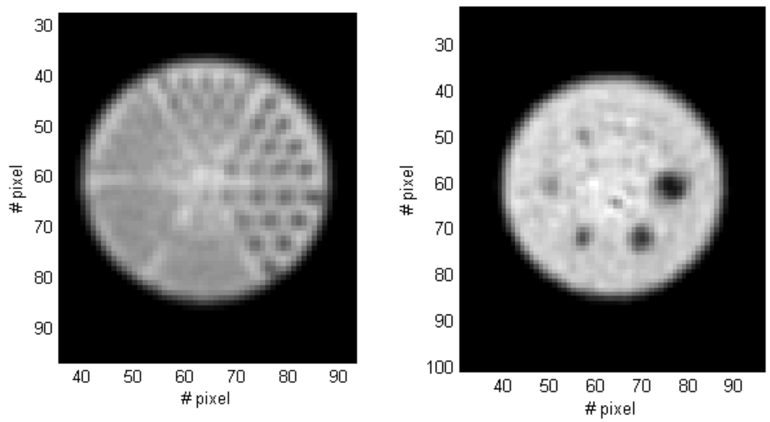

Automatic adaptative orbit
R ~ 17 cm

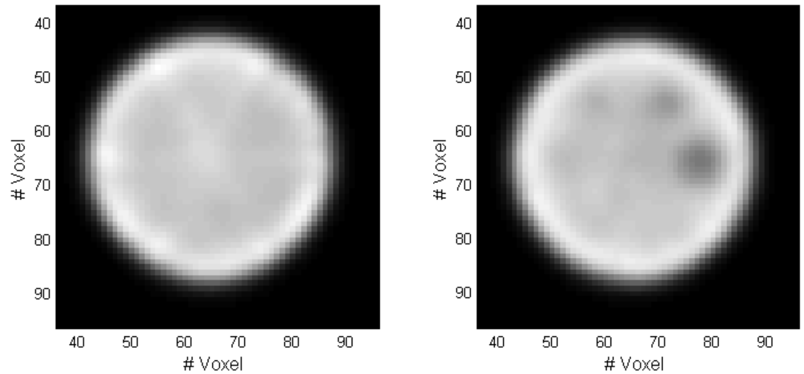

fixed circular orbit
R ~ 30 cm

Being a slim patient is a good idea !!!

SPECT

How many projections are needed ?

Projections are discrete data-sets

Sampling theorem: $\Delta r \leq 1/2k_{max}$

k_{max} = Nyquist freq.

Sampling requirement: $\Delta r \leq FWHM_{PSF} / 3$

Angular sampling requirement
Number of angular views $N_{views} \leq \pi D / 2\Delta r$

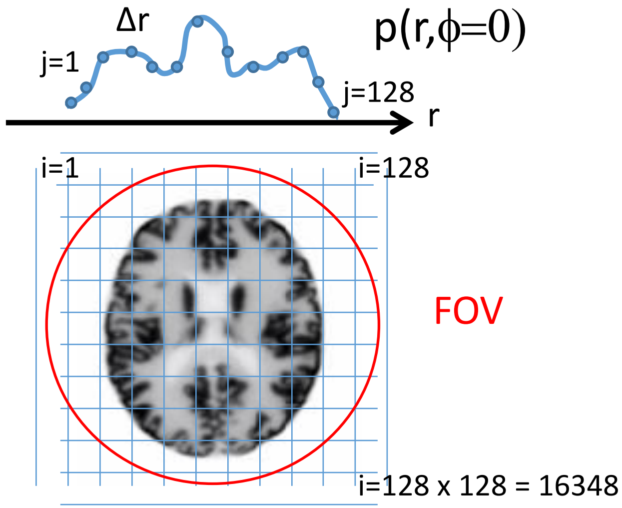

Example

FOV D = 30 cm
FWHM = 10 mm

Linear sampling interval should be : $\Delta r \leq 10/300 \approx 3.3mm$

Number of pixel in the r direction is : 300/3.3 = 90 (~100 samples are needed)
→ typically power of 2 in digital data analysis → projection discretisation in 128 samples (2^7)

Number of views is : (π x 30)/(2x(1/3)) ~ 140 views
→Thus typically 128 angular acquisitions are acquired
→ Reconstruction matrix size = 128 x 128
→ 16348 image pixels

SPECT

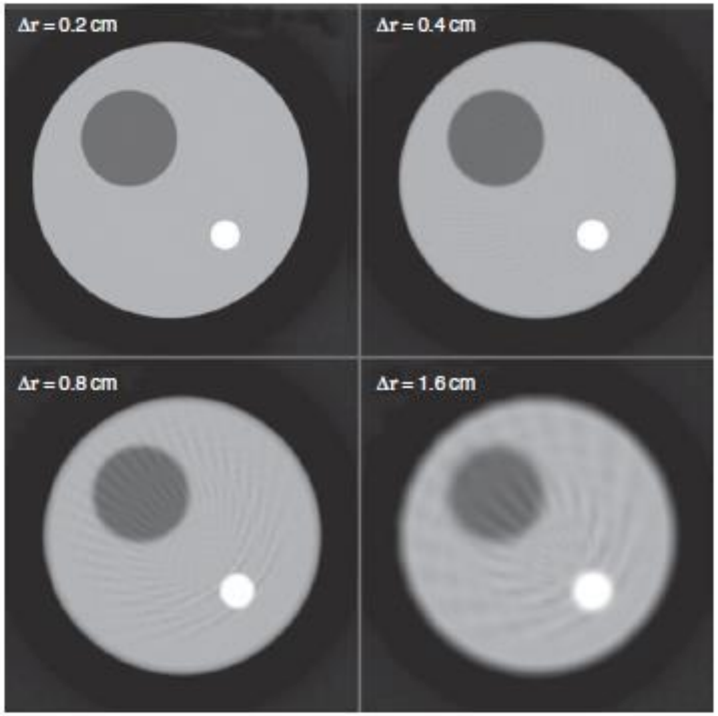

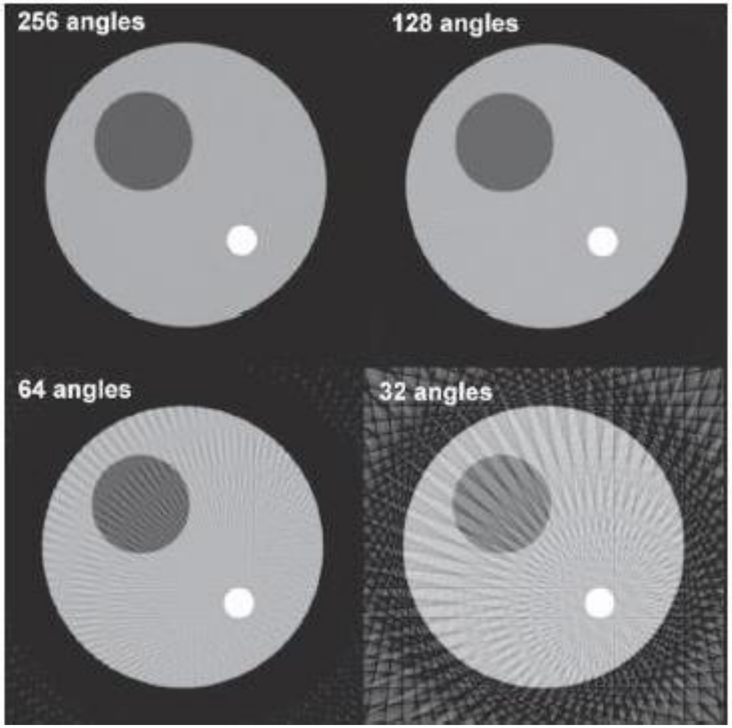

Linear undersampling (Δr)
→Spatial resolution degradation
→Image artifacts

Angular undersampling (N_{views})
→Spatial resolution degradation
→Image artifacts

SPECT

Signal intensity in SPECT voxels is proportional to the amount of activity contained

But absolute quantification (Bq/mL) is very hard to achieve

- **Line of response** are not straight cylinders but are diverging cones
- **Tissue attenuation** results in depleted signal from deeper location in patient
- **Scattering** in patient, detector and collimator results in event mislocalisaton

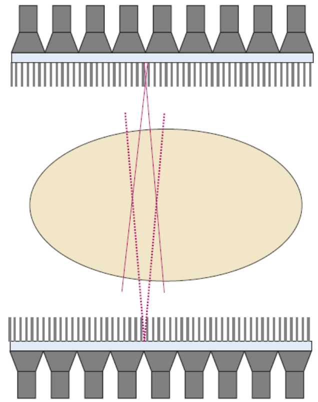

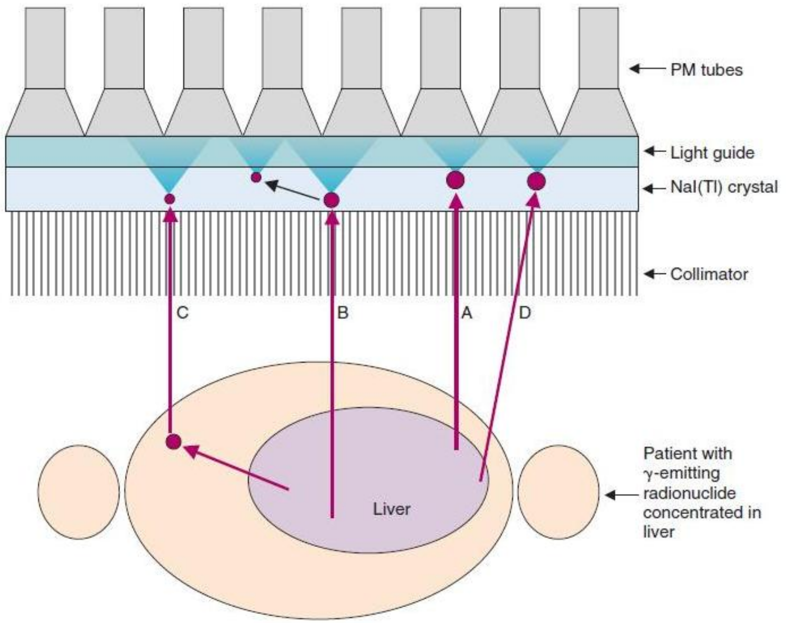

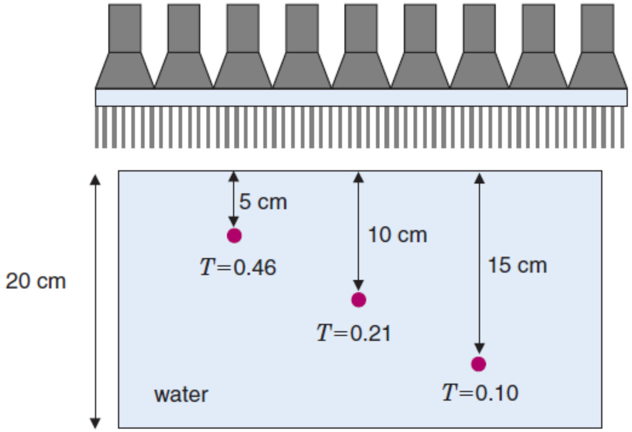

Transmission $T = e^{-\mu x}$
for 140-keV γ rays in water, μ=0.155 cm^{-1}

- An exact **detector collimator response** is needed (septal penetration, PSF resolution recovery)

SPECT

Attenuation correction in SPECT

Attenuation is inverse of transmission $$T = e^{-\mu x}$$

Attenuation coeff. Tissues $\mu_w(E_\gamma)$

- Tissue type
- Gamma Energy

$$\mu_{water}(140keV) = 0.155cm^{-1}$$

$$\mu_{bone}(140keV) = 0.25cm^{-1}$$

Conjugate counting

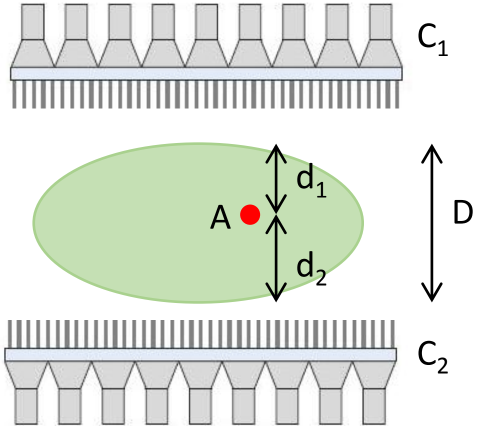

$$C_G = \sqrt{C_1 \times C_2} \qquad C_1 = A \times k \times e^{-\mu d_1} \quad C_2 = A \times k \times e^{-\mu d_2}$$

$$C_G = \sqrt{C_1 \times C_2} = A \times k \times \sqrt{\exp(-\eta(d_1 + d_2))}$$

$$C_G = A \times k \times \exp(-\mu D / 2)$$

Geometric mean

Independent on source depth
→ only depends on total tissue thickness (D)

^{99m}Tc-Line source response
Air

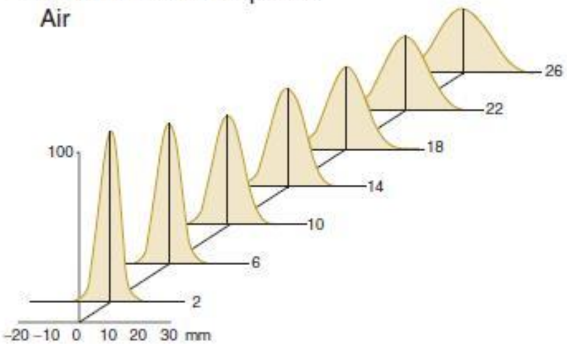

Water

Single detector only

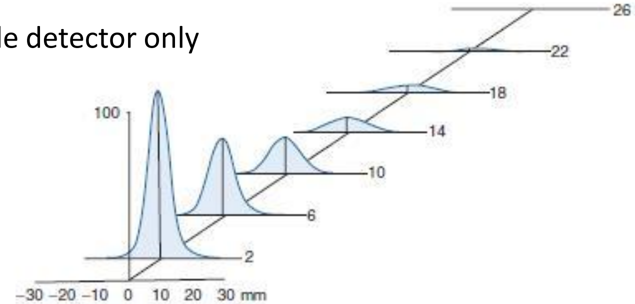

Detector-2

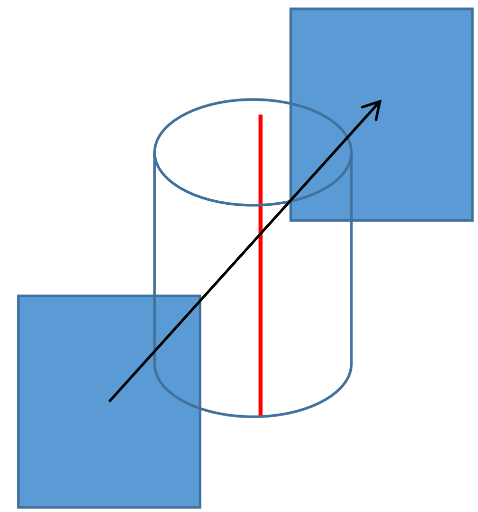

Detector-1

Arithmetic-mean
Air

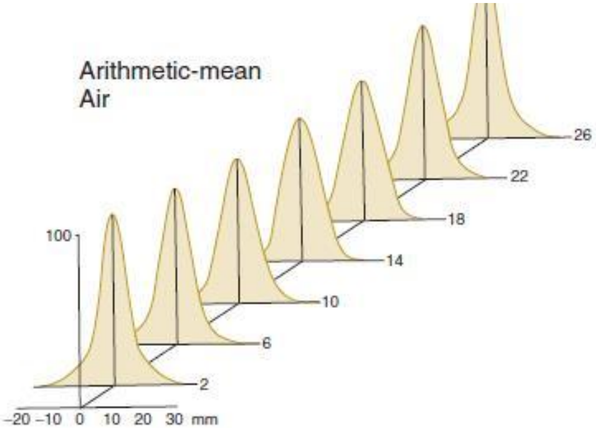

Water

Two opposite detectors
(S1+S2)/2

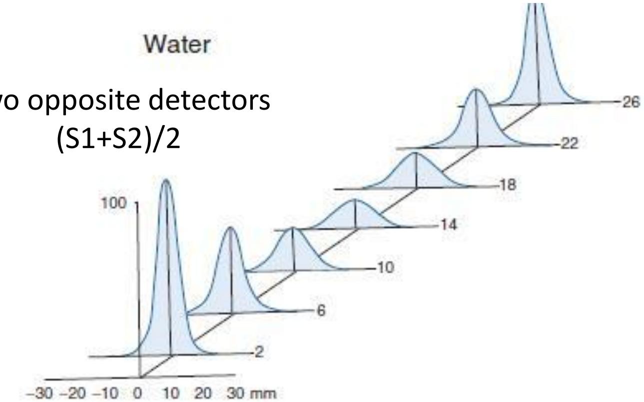

Geometric-mean
Air

$$S_{geom} = \sqrt{S_1 \times S_2}$$

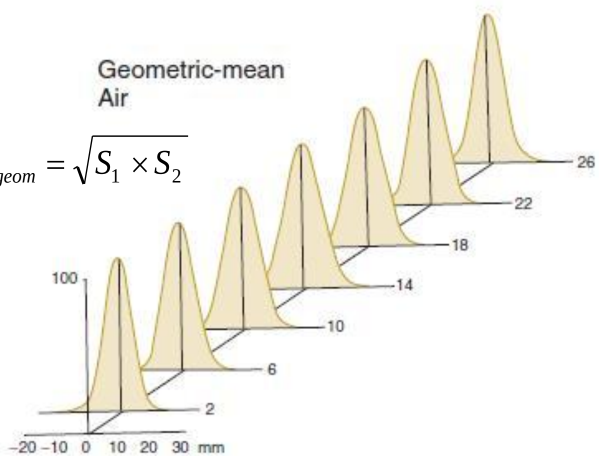

Two opposite detectors

Water

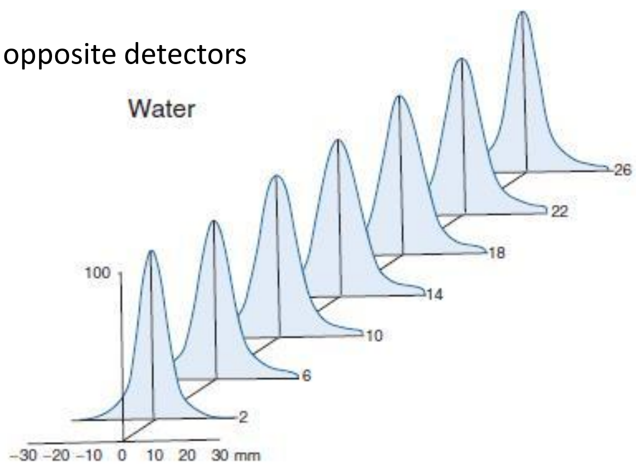

SPECT

Attenuation correction in SPECT

Conjugate techniques applied to projection data (p(r,ϕ))

Geometric mean reduces signal variability in projections

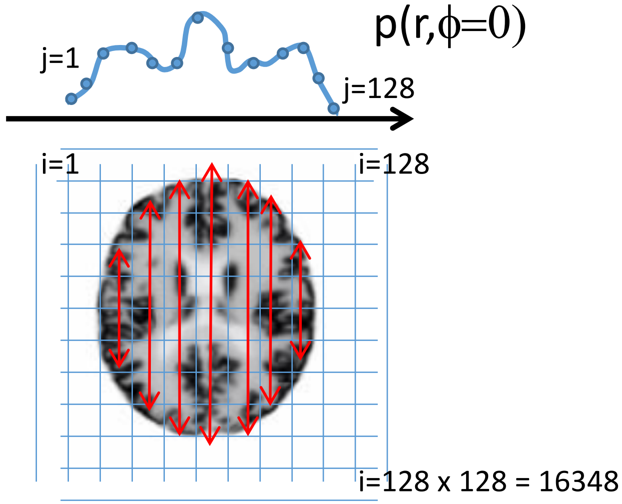

$$p_{geom}^{corr}(r_j,\phi) = \underbrace{\sqrt{p(r_j,\phi)\times p(r_{j'},\phi+180)}}_{\text{Geometric mean}} \times \underbrace{e^{\eta D/2}}_{\substack{\text{Att. Corr. Factor}\\ \text{Along the line of}\\ \text{response}}}$$

Limitations

- ➢ Inaccurate for arbitrary source distribution in FOV
- ➢ Assumption of uniform linear attenuation thought the imaged object

Attenuation correction applied to voxels of reconstructed image (f'(x.y))

1. First uncorrected image estimation: f'(x,y) (ex. by FBP)
2. Estimation of projection path (d_i) along single pixels
3. Correction is applied:

$$f'^{corr}(x,y) = f'(x,y)\times ACF(x,y) \qquad ACF(x,y) = \frac{1}{\frac{1}{N}\sum_{i=1}^{N} e^{-\mu d_i}}$$

Chang's multiplicative method

Limitations

- ➢ Assumption of uniform linear attenuation thought the imaged object

20 cm diam. Cylinder filled with ^{99m}Tc

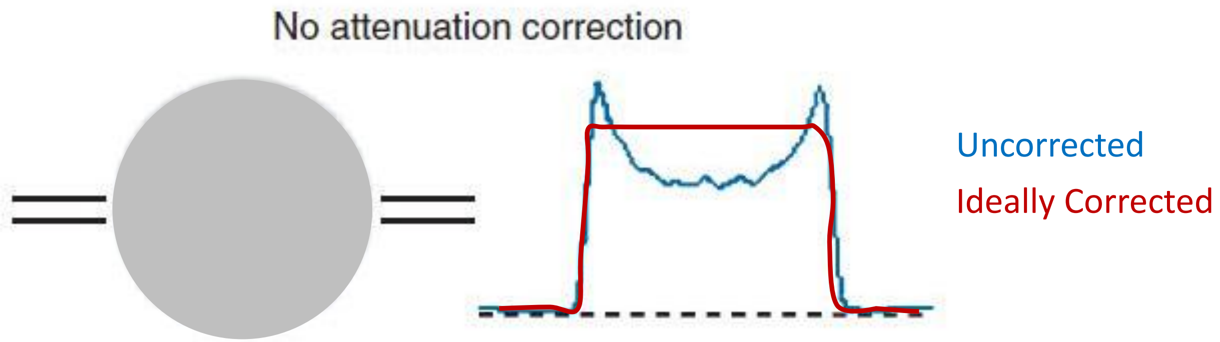

Chang methods are used in commercial SPECT systems
Not accurate enough for absolute quantitation

→Approximation of uniform attenuation coeff. applies to :

- Brain
- Abdomen

Not appropriate for:

- Thorax (lungs)
- Pelvic region (bones)

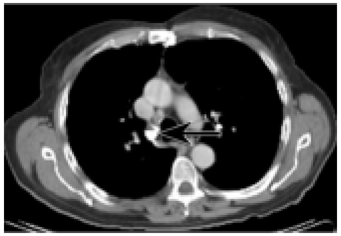

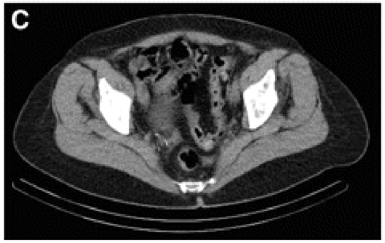

CT based attenuation correction in SPECT

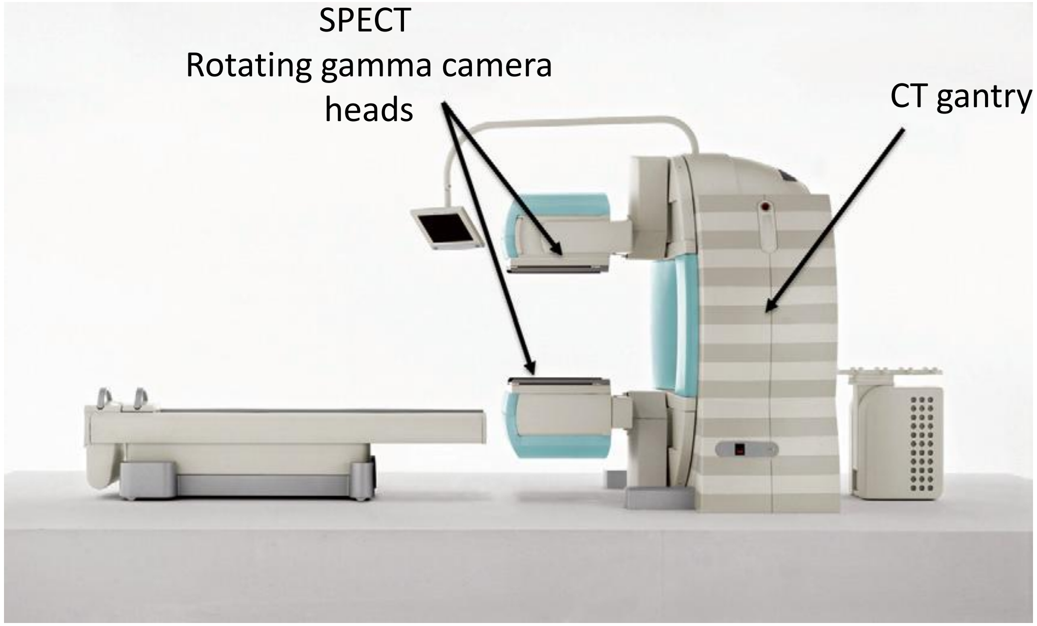

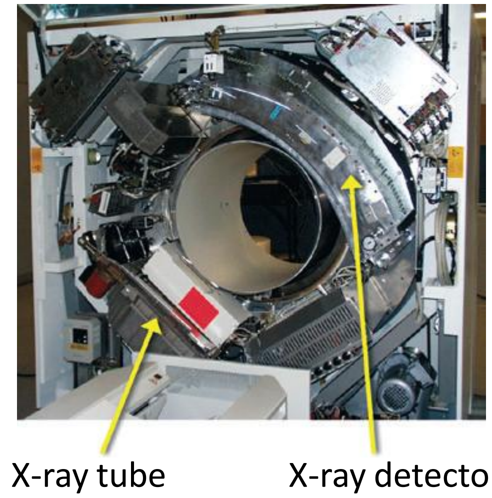

Tissue attenuation can be derived from transmission data (CT)

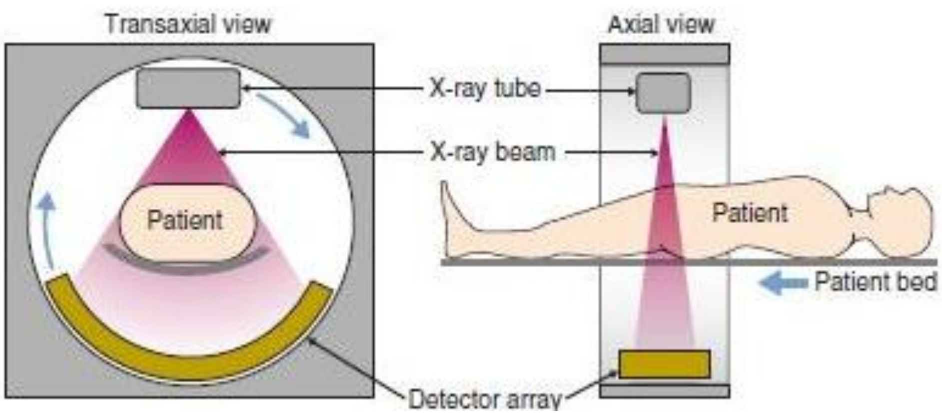

CT-Based
Attenuation map
For attenuation Correction of
SPECT data

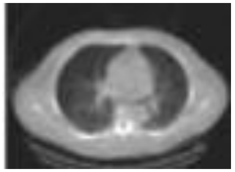

CT-AC is standard in modern hybrid SPECT/CT devices

CT based attenuation correction in SPECT

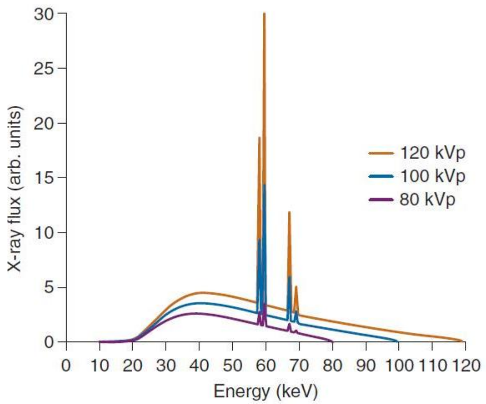

Effective energy of the beam can be defined

120 kVp → 75 keV

Appropriate $\mu(x,y,E\gamma)$ map need:

Energy scaling the attenuation coeff. from effective beam energy to the given radionuclide energy

CT map is in Hounsfield units using a borad-energy Spectrum

Segmentation on CT

- Air
- Bone
- Soft tissues

Attenuation map $\mu(x,y,E\gamma)$

Continuous attenuation map $\mu(x,y,E\gamma)$ from CT

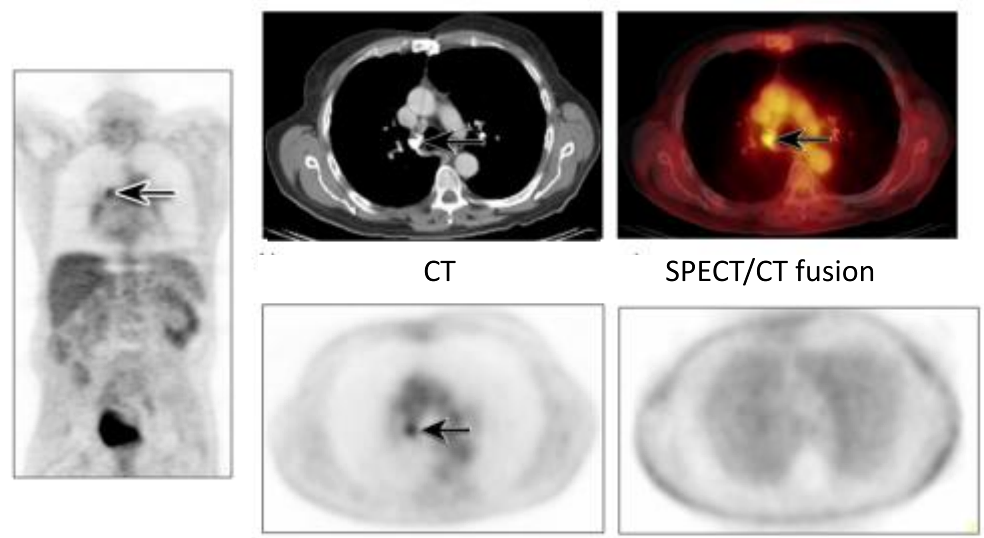

CT

SPECT/CT fusion

AC-corrected SPECT

Non corrected

Scatter correction in SPECT

➢**Scattering** in patient, detector and collimator results in event mislocalisaton

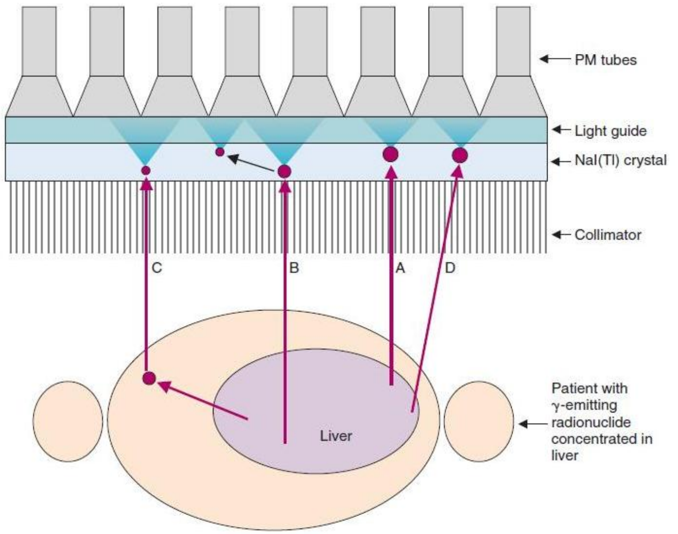

Scatter fraction in the selected energy window in unfavorable condition cab be up to 40%

Scatter correction by Chang corrections → smaller attenuation coefficient
Only works in regions of uniform activity distribution and attenuation

Scatter correction by measured scatter component subtraction in projections

Scatter correction by energy discrimination in PHA

Scatter correction in SPECT
PHA based energy discrimination

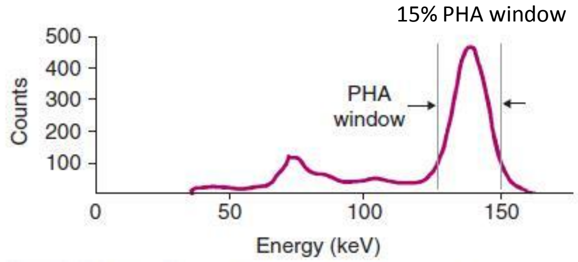

Typical energy spectrum from ^{99m}Tc source (without attenuating/scattering media)

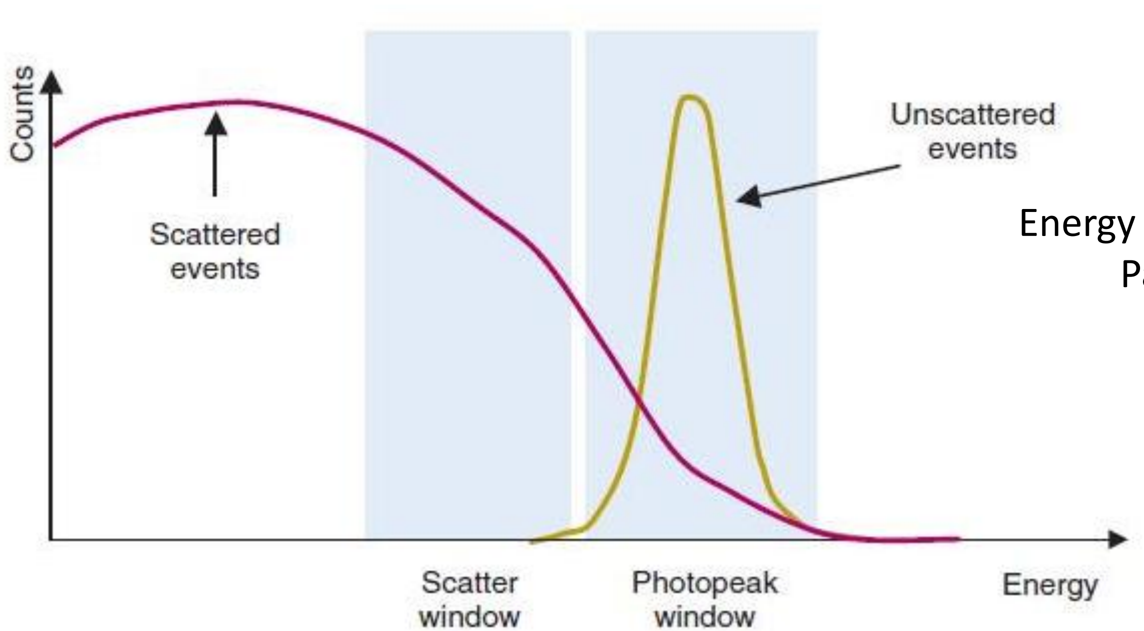

Energy spectrum in the presence of scattering Patient (especially obese patients)

Scatter correction must be performed before Attenuation correction to avoid amplification of scatter contribution

Attenuation and Scatter correction in SPECT
Iterative reconstruction

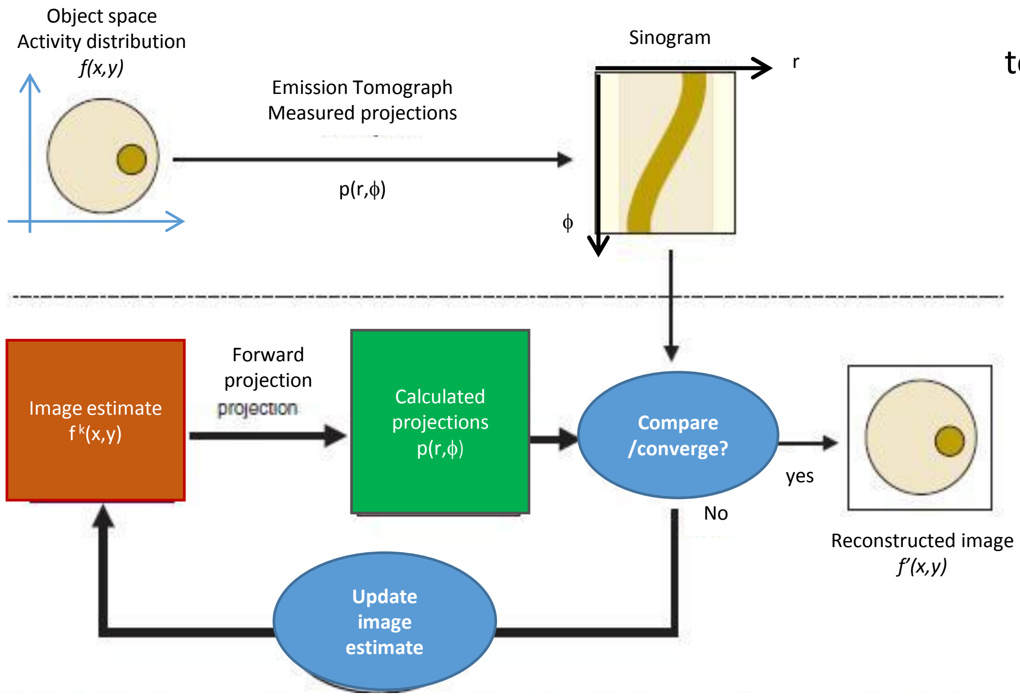

All image pixels (i) have a finite probability ($M_{i,j}$) to contribute to signal intensity into projection data (pj)

$$p_j = \sum_{i=1}^{n} M_{i,j} f_i$$

$$f_i^{k+1} = \frac{f_i^k}{\sum_{j=1}^{m} M_{i,j}} \times \sum_{j=1}^{m} M_{i,j} \frac{p_j}{\sum_{i'=1}^{n} M_{i',j} f_{i'}^k}$$

Attenuating map data can be integrated into the Image Matrix (M)

To account for the probability of scatter radiation in the source region (x,y) to produce a signal into a given detector element (p_j)

Collimator/detector response can also be integrated in M

- Monte Carlo simulations (gold standard)
- Measured data

The way towards
Quantitatively accurate
SPECT imaging

Patient receiving a therapeutic administration
(6 GBq) of Lu-177 DOTATATE

Signal recovery was assessed at organ and lesion level by varying the number of iterations

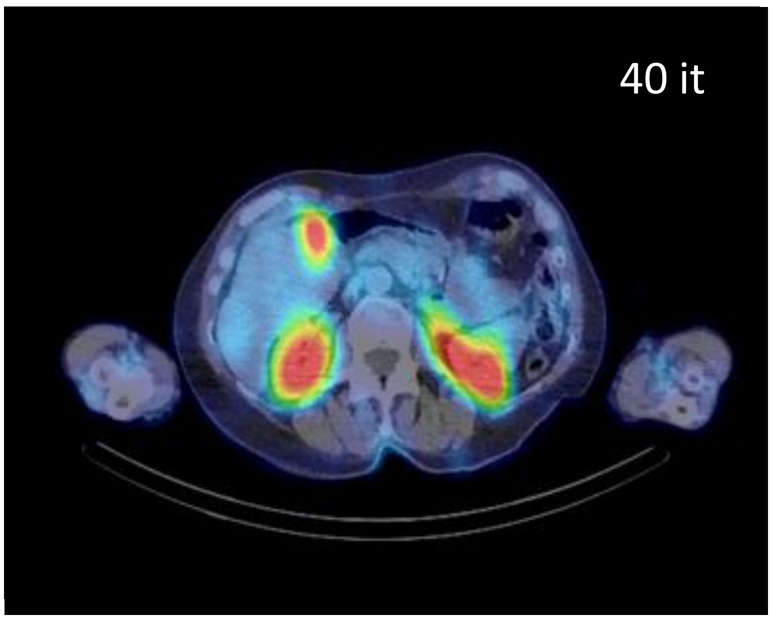

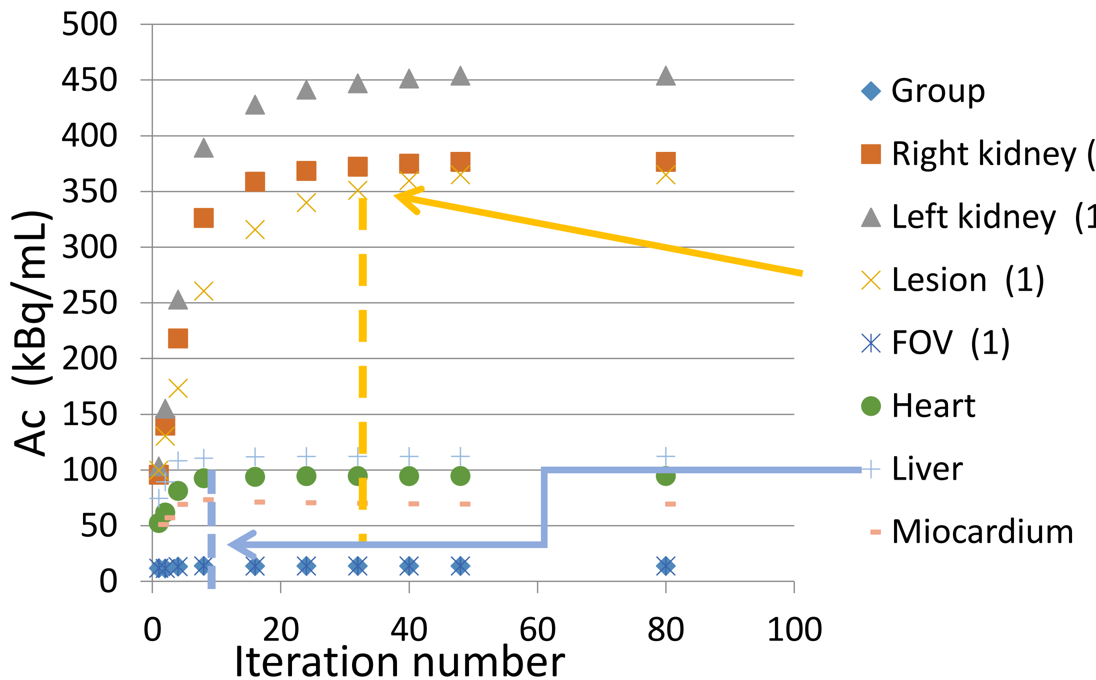

Signal recovery (and convergence) is size dependent

Protocol optimization has a direct impact on organs and lesion dose assessment

Physics in Nuclear Medicine

FOURTH EDITION

Simon R. Cherry
James A. Sorenson
Michael E. Phelps

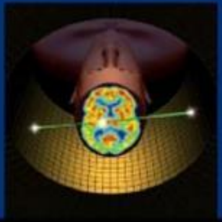

SAUNDERS
ELSEVIER